ASSESSMENT OF API THREAD CONNECTIONS UNDER TIGHT GAS WELL CONDITIONS

A Thesis

by

DWAYNE BOURNE

Submitted to the Office of Graduate Studies of
Texas A&M University
in partial fulfillment of the requirements for the degree of

MASTER OF SCIENCE

August 2009

Major Subject: Petroleum Engineering

ASSESSMENT OF API THREAD CONNECTIONS UNDER TIGHT GAS WELL CONDITIONS

A Thesis

by

DWAYNE BOURNE

Submitted to the Office of Graduate Studies of
Texas A&M University
in partial fulfillment of the requirements for the degree of

MASTER OF SCIENCE

Approved by:

Co-Chairs of Committee,	Jerome Schubert
	Catalin Teodoriu
Committee Members,	Gioia Flacone
	Steven Taliaferro
Head of Department,	Stephen A. Holditch

August 2009

Major Subject: Petroleum Engineering

ABSTRACT

Assessment of API Thread Connections Under Tight Gas Well Conditions. (August 2009)

Dwayne Bourne, B.S., South Carolina State University

Co-Chairs of Advisory Committee: Dr. Jerome Schubert
Dr. Catalin Teodoriu

The modern oil and gas industry of America has seen most of the high quality, easily obtainable resources, already produced, thus causing wells to be drilled deeper in search for unconventional resources. This means Oil Country Tubular Goods (OCTG) must improve in order to withstand harsher conditions; especially the ability of connections to effectively create leak tight seals.

This study investigates the use of thread connections in tight gas fields; therefore, an insight into their potential to contribute to fulfilling the energy demands is necessary. Also, a survey of completed projects done in tight gas fields can provide vital information that will establish the minimum requirements thread connection must meet to perform its functions.

To make suitable adjustments to ensure safe and efficient operations we must thoroughly understand the many aspects of thread connections. To have this understanding, a review of previous works was carried out that highlights the capabilities and imitations of thread connections.

In addition to reviewing previous work done on thread connections; this study measured the viscosity of thread compounds under variable conditions. It was found that viscosity of thread compound falls in the range of 285,667 cP and 47,758 cP when measured between 32.9 ^{0}F and 121.5 ^{0}F. This can be very important because thread compound is essential to the function of thread connections. The knowledge of its viscosity can help choose the most suitable compound. By knowing the value of the viscosity of a thread compound it can also be used to form an analytical assessment of the grooved plate method by providing a means to calculate a pressure gradient which impacts the leakage.

DEDICATION

This thesis is dedicated to my family.

ACKNOWLEDGEMENTS

I would like to thank Dr. Jerome Schubert and Dr. Catalin Teodoriu who served as co-chairs of my graduate committee for their advice, guidance, support and help throughout the research.

I wish to thank Dr. Falcone and Dr. Taliaferro for serving as a member of my graduate committee.

I am grateful to the Crisman Institute and Dr. Stephen Holditch, head of the Petroleum Engineering Department, for funding this research.

I also want to extend my gratitude to Dr. Daulat Mamora, Graduate Advisor in the Petroleum Engineering department, for allowing me the opportunity to conduct my experiments for this study by making his laboratory and equipment accessible. I also thank him for his assistance and ideas during the experimental stage.

Special thanks to all the professors I have had the opportunity to learn from during my coursework here at Texas A&M University and to all the staff members who assisted in fulfilling all administration requirements. This prestigious institution has played an important part in both my personal and professional development.

I also would like to thank my officemates, classmates, and lab mates for their friendship, support and assistance.

TABLE OF CONTENTS

Page

ABSTRACT iii

DEDICATION iv

ACKNOWLEDGEMENTS v

TABLE OF CONTENTS vi

LIST OF FIGURES ix

LIST OF TABLES xii

INTRODUCTION 1

- Background of OCTG 2
- Connection Thread 4
- Thread Profile 5
- Thread Pitch 5
- Thread Shape 6
- Sealing Element 7
- Thread Compound Seal 7
- Polymeric Sealing Ring 7
- Metal-to-metal Shoulder Seal 8
- Pressure Energized Metal-to-metal Seal 8
- Upset 9
- API Tubular Classification 10
- Weight 11
- API Connections Classifications 12
- API Round Thread Casing and Thread Features 12
- API Buttress Thread Casing and Thread Features 13
- API Extreme Line Casing and Thread Features 13
- Approach 14

TIGHT GAS SANDS 16

- What Makes a Tight Gas Reservoir? 16
- Tight Gas Abundance 17
- Production of Tight Gas in the United States 18
- Properties of Tight Gas Reservoirs 20
- Algeria 20
  - Tiguentourine Field 20
  - Ohanet Ordovician Reservoir 21
- Germany 22
  - Söhlingen Field 22
- Mexico 23
  - Arcabuz-Culebra Field 23
- Colorado 24
  - Piceance Basin 1 24
  - Piceance Basin 2 25
  - Wattenberg Field-Denver Basin1 25

Page

Wattenberg Field-Denver Basin2 25
East Texas 26
Trawick Field 26
James Reservoir 27
Carthage Field 28
Data Analysis 30
Overview of Tight Gas Reservoir Properties 36

TESTING THE SEALABILITY OF API THREADS 38

Numerical and Experimental Distribution of Temperature and Stress Fields in API Round Threaded Connection. 38
Analysis of Simulation Results 39
Experimental Study 39
Results of Experimental Study 40
Investigation of API 8 Round Casing Connection Performance 41
Finite Element Models Solution 42
Strain Gage Test Connection 43
Stresses and Criteria 44
Sealability and Torque 44
Assembly Torque 45
Effects of Axial Tension and Internal Pressure on Assembly Torque 46

TESTING API THREAD COMPOUNDS 47

The Role of Thread Compounds 47
Tightness Testing 48
Grooved Plate Method 50
Slot Flow Theory 52

TESTING THE VISCOSITY OF THREAD COMPOUNDS 54

Experiment 54
Thread Compound Samples 54
API Modified Thread Compound 54
NCS-30 55
Kopr-Kote 56
Equipment 56
Brookfield DV-III Ultra Programmable Rheometer 56
Brookfield Refrigerated Temperature Bath 58
Thermolyne Furnace 30400 59
Procedure 60
Basic Procedure 61
Fatigue Tests 62
Constant Temperature Tests 62

RESULTS AND ANALYSIS 63

Viscosity Measurements 63
API Modified 63
NCS-30 67
Kopr-Kote 72
Fatigue Tests 76
Constant Temperature Tests 79

Page

Analysis Using Slot Flow Approximation 79

CONCLUSIONS AND RECOMMENDATIONS 81

Conclusions 81
Recommendations 83

REFERENCES 84

NOMENCLATURE 88

APPENDIX A 90

VITA 94

LIST OF FIGURES

Page

Fig. 1 – Helical paths of round thread connections 1

Fig. 2 – Cross section of (a) coupled connection and (b) integral connection 4

Fig. 3 – Cross section of thread profile showing (a) conical form (b) conical and cylindrical form and (c) cylindrical form 5

Fig. 4 – Thread pitch areas 6

Fig. 5 – Thread shape 6

Fig. 6 – Posssible position for sealing rings (modified from Vega Navarro 2004) 7

Fig. 7 – Types of metal-to-metal shoulder seals 8

Fig. 8 – Display of various types of metal-to-metal seals 9

Fig. 9 – Upsetting possibilities 9

Fig. 10 – API non upset casing round thread 12

Fig. 11 – API buttress thread casing 13

Fig. 12 – API extreme line casing 14

Fig. 13 – Resource pyramid showing distinctions between conventional and inconventional resources 17

Fig. 14 – A comparison of low quality fluids and permeability 18

Fig. 15 – Resource pyramid for tight gas classification in the U.S. 19

Fig. 16 – Tight gas basins in the U.S. 20

Fig. 17 – Well plan of wells drilled in the Ohanet Ordovician reservoir 21

Fig. 18 – Well measurements of a well in the Piceance Basin 24

Fig. 19 – Measurements of a well in the James Reservoir 27

Fig. 20 – Completion design for a well in Pirkle #2 30

Fig. 21 – Bar chart comparing reservoir pressures 32

Fig. 22 – Scatter plot of reservoir pressure 33

Fig. 23 – Reservoir temperatures of some tight gas fields across the world 34

Fig. 24 – Scatter plot of reservoir temperatures 34

Page

Fig. 25 – Depth of tight gas sands 35

Fig. 26 – Scatter plot of reservoir depth of tight gas fields 36

Fig. 27 – Pictures of field tubing thread showing galling 38

Fig. 28 – Axial stress of the threaded model, unthreaded model, and straing gauge tests at different positions of the connection 43

Fig. 29 – Contact pressure for assembly, assembly plus tension, and assembly plus tension plus pressure 45

Fig. 30 – Graph showing torque values along the connection 46

Fig. 31 – Classification of thread compounds used in tests by use and toxicity 48

Fig. 32 – Picture of test apparatus showing simulated pipe connection 49

Fig. 33 – Results of the tightness tests 50

Fig. 34 – Pictures of the grooved (top) and seal (bottom) plates 51

Fig. 35 – Graph showing leak pressure as a function of contact pressure 52

Fig. 36 – Brookfield DV-III Ultra 58

Fig. 37 – Brookfield Refrigerated Temperature Bath 59

Fig. 38 – Thermolyne Furnace 30400 60

Fig. 39 – Graphical representation of viscosity measurements 65

Fig. 40 – Forecasted viscosity data 66

Fig. 41 – Graph displaying viscosity as a function of shear stress 66

Fig. 42 – Graph showing viscosity against torque 67

Fig. 43 – Viscosity as a function of temperature 69

Fig. 44 – Forecast of viscosity data 70

Fig. 45 – Viscosity as a function of shear stress 71

Fig. 46 – Viscosity as a function of torque 71

Fig. 47 – Viscosity as a function of temperature 73

Fig. 48 –Forecast of viscosity data for Kopr-Kote 74

Fig. 49 – Viscosity against shear stress 75

Fig. 50 –Viscosity against torque 75

Page

Fig. 51 – Graph showing viscosity as a function of no. of cycles 77

Fig. 52 – Graph showing results from the second fatigue tests 78

Fig. 53 – Transformation from annular flow to slot flow (modified from Bourgoyne et. al)..... 90

Fig. 54 – Free body diagram for fluid element in a narrow slot 91

LIST OF TABLES

Page

Table 1 –Comparison of the advantages and disadvantages of each type of connection. 3

Table 2 – Comparison of yield and tensile strength of different grades of steel (modified from Vega Navarro 2004) 11

Table 3 – Reservoir properties of Tiguentourine Field 21

Table 4– Well measurement of an Ohanet Ordovician vertical well. 22

Table 5 – Well measurement of an Ohanet Ordovician horizontal well 22

Table 6 – Reservoir properties of the Travis Peak formations 27

Table 7 – Completion design for a Carthage Field well 29

Table 8 – A collection of all reservoir properties reported 31

Table 9 – Summary of reservoir properties 36

Table 10 – API and test connection thread dimensions 41

Table 11 – Hand calculated contact pressures and stresses at the pin end, box end and centre of the connection 42

Table 12 – Composition of API-modified thread compound 47

Table 13 – Display information of Brookfield Rheometer 57

Table 14 – Results of viscosity measurements 64

Table 15 – Average readings from rheometer 65

Table 16 – Measurements from the experiments performed on NCS-30 68

Table 17 – Average values from viscosity experiments 69

Table 18 – Results from viscosity experiments on Kopr-Kote 72

Table 19 – Average values from viscosity measurements 73

Table 20 – First set of fatige test results 76

Table 21 – Second set of results from fatigue tests 78

Table 22 – Results from the tests with temperature held constant 79

Table 23 – Input data for slot flow approximation 80

Page

Table 24 – Results from the slot flow approximation for round thread 80

Table 25 –Results from the slot flow approximation for buttress thread 80

Table 26 –Summary of viscosity results 82

Table 27 – Viscosity of thread compound at average reservoir temperature 82

INTRODUCTION

American Petroleum Institute (API) round thread connections have been extensively used for "low cost" wells mainly because they are cheap, simple, and easy to manufacture[1]. Their two main functions are to provide structural integrity by keeping the pipe sections attached to form a continuous length and to provide sealing integrity by maintaining leak tightness against internal and external fluids while subjected to loads of assembly interference, axial tension or compression, internal and external pressures, and bending[2].

The sealing mechanism of API round thread includes the use of thread compound which is used to dam leak passages. These leak passages shown in **Fig. 1** are helical capillaries found at the roots and crests of the thread tooth and vary in area according to the size of the thread tooth as well as thread tolerances. Badiciu and Teodoriu (2007) have reported areas between 0.0490 mm^2 to 0.1555 mm^2. Fluid leakage in thread connections occurs under a pressure differential across the leak passages or the absence of thread compound. It is harder to create a leak tight connection when the fluid to be seal is a gas because of its low surface tension and viscosity. Some gases can also enter the leak passage and breakdown the thread compounds rendering them unable to create a leak-tight connection.

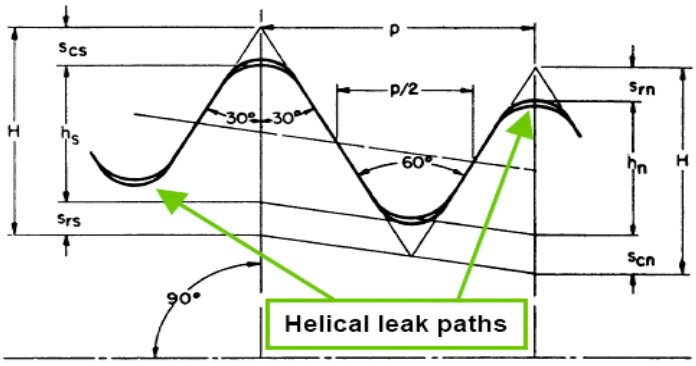

Fig. 1 – Helical paths of round thread connections[3]

This thesis follows the style of *SPE Production and Facilities.*

To fully understand thread connections we must identify the various characteristics of Oil Country Tubular Goods (OCTG) which directly play a role in the sealing process. The following section is a description of the many mechanisms involved with thread connections.

Background of OCTG

Oil Country Tubular Goods (OCTG) comprises the casing and tubing of wells, where the most problematic element is connections. Connections provide casing and tubing with fluid sealing and mechanical resistance and also involve stop shoulders. In today's progressive drilling to lower depths, with higher temperature and pressure, the need for more innovative connection design increases for successful drilling operations and long life production or injection of the well.

The downhole connection, from the beginning of rotary drilling, joins two tubulars together. Some connections may need to provide sealing for water or oil only, but some may need to be gas tight, as well, and to withstand external loading like high temperature, pressure, and mechanical pressure.

Connections possess a complex mechanical design and geometry such that minute changes to their construction and geometric parameters can result in varying connection characteristics and performance capabilities. The best combination of these parameters will improve the load distribution, and thus the fatigue resistance of the connections. The simplest of these parameters, that can be adjusted, are the dimensional configuration of the connections. These are outer diameter (OD), inner diameter (ID), coupling outer diameter (COD), make up loss (MUL), wall thickness (t), and length of coupling (N_L).

Threaded connections have two distinctive types: coupling connections and integral connections. **Table 1**[4] compares the advantages and disadvantages of integral and coupling connections. **Fig. 2**[4] shows a simple drawing depicting examples of a coupling connection and integral connection.

Table 1 –Comparison of the advantages and disadvantages of each type of connection[4]

	Coupled Connection Both ends of the tubular are constructed as pin threads. The pins are then joined together with the help of a double box thread (coupling).	**Integral Connection** One end of the tubular is constructed as a pin thread and the other end as a box thread and the two ends are joined together
Advantages	Upsetting not necessary Easy to repair Bigger critical area Strong shoulder stop for axial forces and torque Long sleeve option for higher strength Higher pitch (taper) and depth of groove possible	Allows only one joint every two pipes and only two threads Smaller connection OD Flexibility to bend in deviated boreholes Fully flush option Efficient flow Easy to repair (without upset)
Disadvantages	Pipe diameter increases Obstruction of hole wall while running Requires two joints for every two pipes and four threads Bigger connection outer diameter (OD)	Upsetting necessary in most cases Complicated to repair if upset Pitch lamination: minimum thickness on the peak required Smaller critical area

(a)

(b)

Fig. 2 – Cross section of (a) coupled connection and (b) integral connection[4]

Connection Thread

Connection threads have two main functions. They are to join two pipes together and to transfer acting forces from one pipe to another[4]. The type of thread will determine the connection life. Five parameters can be changed to produce different types of threads:

Size: influences the make-up time (make-up loss) and the axial load capacity

Load flank angle: influences the conversion from axial to radial loading

Taper: prevents the joint from unscrewing under its own weight

Pitch: influences the assembly time, controls cross-threading

Thread Profile: determines the load response of the connection[4]

These parameters can be classified into three groups

Thread profile

Thread pitch

Thread shape

Thread Profile

Thread forms may be conical, cylindrical, or a combination of the two. Conical form is the most popular because of its economical construction, accepted capabilities, resistance to tensile separation and wide range of implementation. In general, thread form regulates the cross sectional area of the pin and the box and enables the connection to withstand axial loads without separating. **Fig. 3** shows a cross section view of each thread profile.

(a)

(b)

(c)

Fig. 3 – Cross section of thread profile showing (a) conical form (b) conical and cylindrical form and (c) cylindrical form[4]

Thread Pitch

The thread pitch is the height of the unwinded thread line parallel to the thread axis[4]. **Fig. 4** shows different pitch areas at different points along the pin.

1: Increased pitch area

2: Standard pitch area

3: Decreased pitch area

Fig. 4 – Thread pitch areas[4]

Thread Shape

The thread shape shown in **Fig. 5**[4] describes the shape of the thread tooth by the size of the dimensions such as the tooth height, tooth length, stab flank angle, and load flank angle. The stabbing flank angle, α is at the bottom of the thread; the load flank angle, β is at the top; and the tooth angle, γ is formed at the end of the thread. Thread tooth form is designed to withstand different loading situations.

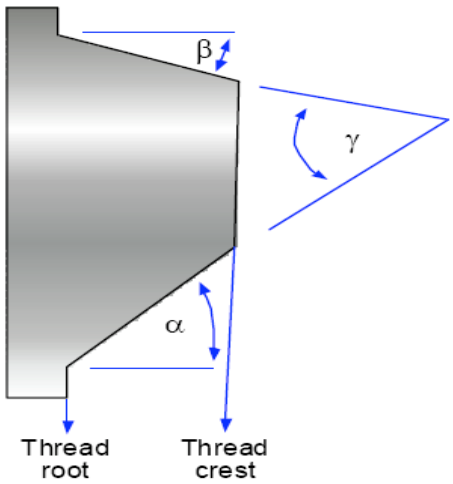

Fig. 5 – Thread shape[4]

Sealing Element

Casing and tubing connections need to be impenetrable by fluids from the reservoir; therefore, the sealing mechanism must withstand internal and external axial loads. Four types of sealing mechanisms are used: metal-to-metal seal, shoulder seal, elastic ring, and thread seal**.**

Thread Compound Seal

This type of seal uses a dope filling between the pin and the box thread that dams the leak passage to maintain fluid pressure. Gases that decompose the doping will compromise the seal. Therefore thread seals are generally applicable only for liquid sealing.

Polymeric Sealing Ring

The seal ring should be activated during the makeup procedure. The ring would be sanded down with the pin thread to provide a pressure sealing between pin and box. Polymeric rings cannot be applied on every environment, such as high temperatures and pressures. The seal ring can be positioned along the thread or near the external or internal shoulders and should be removed and renewed before every make up procedure and have no cracks or splits[3]. **Fig. 6** shows a cross section of an integral connection showing possible positions of sealing rings.

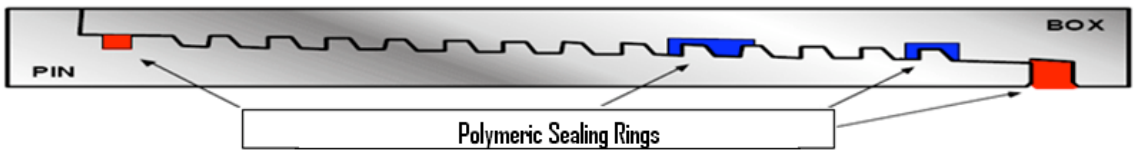

Fig. 6 – Posssible position for sealing rings (modified from Vega Navarro 2004)

Metal-to-metal Shoulder Seal

The shoulder seal is used as a preventative measure, as it provides a secondary seal to the metal-to-metal seal and hydraulic seal and ensures the pin and box are connected correctly. The shoulder could be internal, external, and/or intermediate and can be activated with high pressure[4]. Internal shoulder seals are formed on the pin side of the connection, external shoulder seals are formed on the box side of the connection, intermediate is formed at neither side, and the pin to pin shoulder is formed by the pins of a coupling connection pressing against each other. **Fig. 7** displays examples of the different types of shoulder seals.

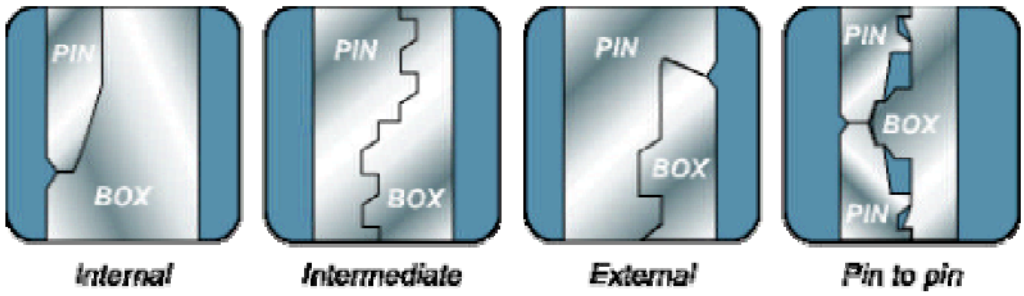

Fig. 7 – Types of metal-to-metal shoulder seals[4]

Pressure Energized Metal-to-metal Seal

Metal-to-metal seals are used near the connection ID to seal internal fluid pressure and contain or to exclude drilling, production, or treatment fluids. This type of seal, located at the end of the pin, the middle of the pin, or at the upper pin-box contact is brought about by the application of torque to the threads of the connection, bringing the box and pin together at high pressure. The pressure generated should be more than the expected internal pressure to create a gas-tight seal. **Fig. 8** shows how both metal ends connect with each other.

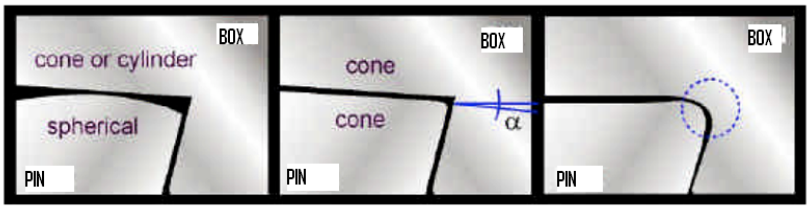

Fig. 8 – Display of various types of metal-to-metal seals[4]

Upset

Upset is the ending part of a tubular constructed with different thicknesses. This controls wall thickness, outer and inner diameter and strength of connection. Some possibilities are:

Non-Upset

Internal Upset

External Upset

Internal & External Upset[4]

Fig. 9 displays the look of the tubular with each type of upset.

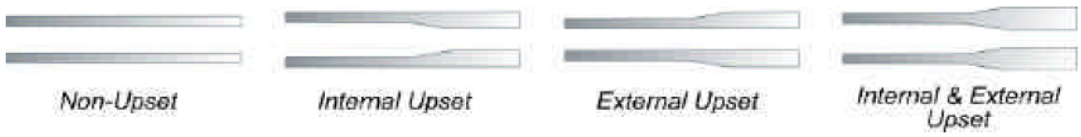

Fig. 9 – Upsetting possibilities[4]

One of the factors that also determine the strength, thickness and environment of the connection is the type of material used. Pipes made of higher quality materials can be thinner and have the same strength as thicker pipes of lower quality material[4]. For environments containing H_2S, steel that has fine-grained homogeneous structure and low non-metallic content can prevent hydrogen atoms from reacting with the H_2S. The H_2S causes cracks at stresses below the strength limit of the material.

A connection must withstand many different loads that are applied because of external conditions. These include tension loads, axial compressive stress, torsion, bend, cyclic stressing, superimposed stresses, temperature and corrosion. To accommodate these load situations the optimal connection must be chosen.

API Tubular Classification

API specifies the specifications, such as the physical dimensions, internal and external upsets, size, weight, grade, and properties the material of the majority of tubular goods manufactured. The classification according to API 5T standards characterizes the dimensions of the pipe body, the grade of steel and the dimensions and style of the connection. The grade of steel defines the pipe's yield strength. The grade is quoted as a letter and a number separated by a hyphen. The higher the letter is the higher the yield strength. The number represents the minimum yield. Steel may be normal, high-strength, or limited.

Normal Steel. The tubular is seamless or electrically welded with no addition of extra metal and undergoes heat treatment. Maximum phosphate content is 0.04% and sulphur is 0.06%[4].

High Strength Steel. The tubular is seamless. Phosphate and sulphur values are the same as normal steel[4].

Limited Yield Strength Steel. The tubular is seamless or electrically welded with no additional metal and undergoes heat treatment. Limited strength steels contain 0.05% carbon, 0.04% phosphorous, 0.06% sulphur, 0.35% silicon and may contain manganese, molybdenum, chromium, nickel, or copper[4].

Table 2 below shows the different types of steel and a range of values of the yield strength and tensile strength which is associated with each type.

Table 2 – Comparison of yield and tensile strength of different grades of steel (modified from Vega Navarro 2004)

		Yield Strength				**Tensile Strength**	
	Grade	Minimum		Maximum		Minimum	
		kpsi	Mpa	kpsi	Mpa	kpsi	Mpa
Normal Steel	H40	40	276	80	552	80	414
	J55	55	379	80	552	75	517
	K55	55	379	80	552	95	665
	N80	80	552	110	758	100	689
High Strength Steel	P105	105	724	135	931	120	827
	P110	110	758	140	965	125	827
	Q125	125	862	155	1069	135	931
	V150	150	1034			160	1104
Limited Yield Strength	C75	75	517	90	620	95	655
	L80	80	552	95	655	95	655
	C90	90	620	105	724	100	690
	C95	95	655	110	758	105	723

Weight

The weight of a pipe can be measured using the following equation[4]:

$w_L = (w_{pe}L) + e_w$ …… (1)

where w_L is the calculated weight of a pipe of length L in lb, w_{pe} is the plain end weight in lb/ft, L is the length of pipe including end finish in ft, and e_w is the weight gain or loss due to end finishing in lb. For a plain end pipe $e_w = 0$.

To calculate the plain end weight the following equation is used[4:]

$W_{pe} = (OD - t) \times t \times 10.679255$ ……..……..……..…….(2)

where OD is the outer diameter of the pipe, and t is the thickness in inches.

Other important classifications of pipes are the range and diameter. The range is the length of the section of pipe and the diameter refers to the outer, inner and drift diameter of the pipe. The drift diameter is the diameter of a gauge that is capable of passing through the pipe.

API Connections Classifications

The API classifies three types of connections by their thread tooth form.

API casing round thread

API buttress thread casing

API extreme line casing thread

API Round Thread Casing and Thread Features

This type of connections comes in either long or short thread. It is externally threaded on both ends and uses non upset pipe. The thread profile has rounded crests and roots, and a flank angle of 30^0 to the vertical. It has 8 threads per inch and a 6.25% taper[4]. The API round thread provides hydraulic leak tight connections as long as the leak passage is blocked. This is normally done with a thread lubricant. The API 8-round thread has two leak passages, one between the pin thread crest and box thread root and the other between the pin thread root and box thread crest. **Fig. 10** shows a drawing of the dimensions and shape of API round thread casing.

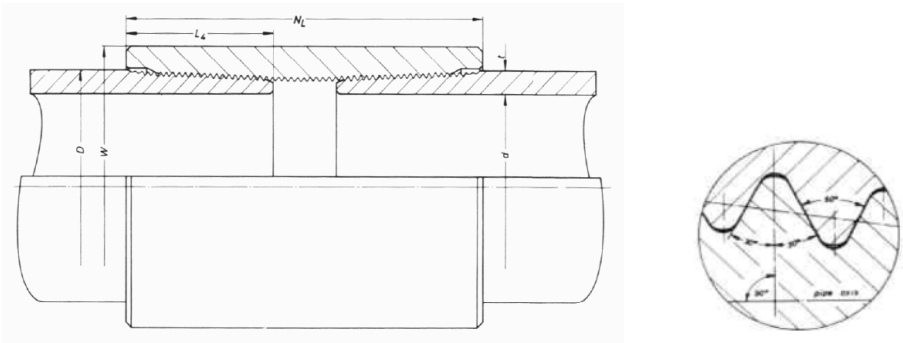

Fig. 10 – API non upset casing round thread[4]

API Buttress Thread Casing and Thread Features

The buttress thread is externally threaded on both ends of a non-upset pipe. The single lengths are joined with an internally threaded regular coupling. The thread profile has flat crests and roots. There are 3^0 and 10^0 angles to the vertical axis of the pipe. There are 5 threads per inch with a 6.25% taper for sizes 13 3/8 inches and smaller. For casing 16 inches and larger a taper of 8.33% is used[4]. **Fig. 11** shows a drawing of API buttres thread casing displaying its dimensions and shape.

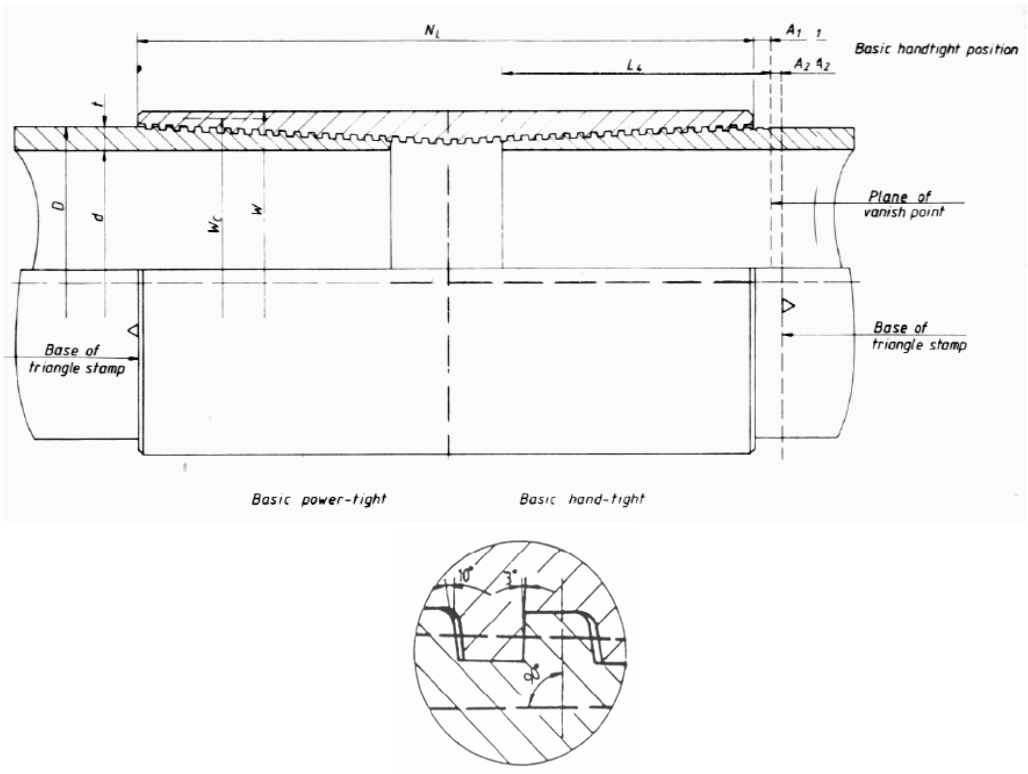

Fig. 11 – API buttress thread casing[4]

API Extreme Line Casing and Thread Features

This thread is internally and externally threaded on internal-external upset pipe ends. The thread profile has flat crests and roots and 6^o flank axis with vertical. It is sealed with a metal-to-metal seal at the pin end and

an external shoulder. The taper is a 1-1/2 in/ft on casing sizes between 5 and 7-5/8 inches. A 7 5/8 in/ft on casing sizes between 8-5/8 and 10-3/4 in[4]. **Fig 12** shows the dimensions and shape of API extreme line casing.

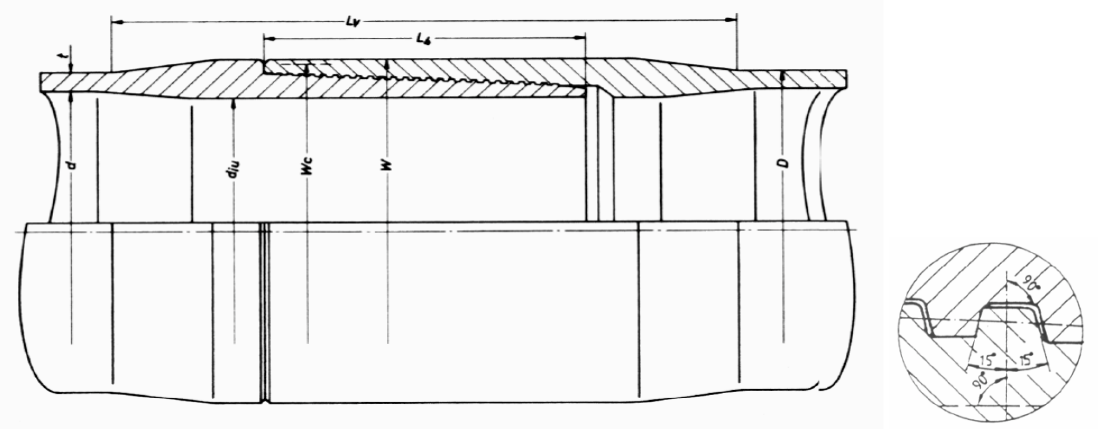

Fig. 12 – API extreme line casing [4]

Approach

A literature review of the work done on API connections was done. This review identified several experiments and studies done on API connections to determine the limits of their capabilities. The review covers simulations done on API connections using Finite Element Method (FEM) analysis and the importance of their findings. It identified several experiments carried out on the connections to get an idea of the pressures API connections are able to seal. Experiments conducted to test the performance of thread compounds were also reviewed.

In order to make use of API connections when drilling wells in tight gas reservoirs we must have an idea of the type of conditions present in these types of reservoirs. To answer these questions published data from several drilling projects undertaken in tight gas reservoirs from around the world were reviewed and a focus on reported reservoir properties and drilling plans were highlighted.

Next, some viscosity measurements were conducted on several samples of thread compounds to identify actual values for thread compound at certain conditions following the guidelines set down by ASTM D 2196 (American Society of Testing and Materials). This information will be useful in predicting the behavior of the thread compound inside the helical paths within the connection.

TIGHT GAS SANDS

What Makes a Tight Gas Reservoir?

A tight gas reservoir can be defined as a reservoir that cannot be produced at economic flow rates nor recover economic volumes of natural gas unless the well is stimulated by a large hydraulic fracture treatment or produced by use of a horizontal wellbore or multilateral wellbores[5]. The tightly packed reservoir, mainly sandstone, does not allow for movement of fluid because a low permeability usually below 0.1mD[6] is associated with tight gas sands. We can calculate the flow through porous media by using the Darcy's Law[7] calculated using **Eq. 3.**

$$pwf^2 = \bar{p}^2 - 1{,}422\frac{\mu_{\bar{p}} z_{\bar{p}g} T q_g}{kh}\left[\ln\left(\frac{r_e}{r_w}\right) - 0.75 + \left(s + D|q_g|\right)\right] \quad \text{(3)}$$

Rock properties are mostly responsible for low permeability of these reservoirs. These poor reservoirs were formed from the lithification of very fine materials such as sand and silts in deep basinal site or over-bank levees. In the United States these depositional settings are usually high-energy settings where the intergranular pores have been largely occluded by authigenic cements (mainly quartz and calcite) [8].

Apart from the very low permeability, there are certain characteristics that are generally present in tight gas reservoirs. Each one may not be present in the same reservoir, but they are all found in some combination in the various tight gas reservoirs around the world:

- Significant formation thickness
- Isolated reservoirs inside the same formation
- Hard to detect or non-existent water transition zones
- Independent Free Water Level for every reservoir
- Over-pressurized reservoirs

- "Anomalous" water gradients
- Water saturation below expected or usual capillary pressure curves interpretation
- Co-existence or intercalation of source rock with reservoir rock[6]

Tight Gas Abundance

A concept called the resource triangle describes the situation where the presence of natural resources follows a lognormal distribution. Here the highest quality minerals are easily developed, but are only present in small amounts. In today's oil and gas industry formations of this type produce conventional resources, where conventional technology end equipment are sufficient to produce volumes at economic flow-rates. Conversely, unconventional resources require the use of various forms of technology such as improved proppants, proppant flowback control, and slimhole drilling and completion techniques to produce economically. The relationship between the improved technology and the quality of minerals are shown in **Fig. 13**[9].

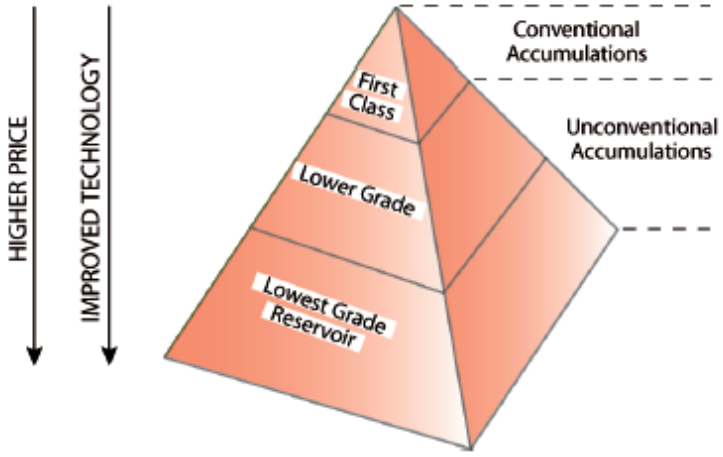

Fig. 13 – Resource pyramid showing distinctions between conventional and inconventional resources[9]

Tight gas is only one form of unconventional resource. Coalbed methane, gas shales, and gas hydrates are the other types that are produced. **Fig. 14** shows how the resources are related to permeability.

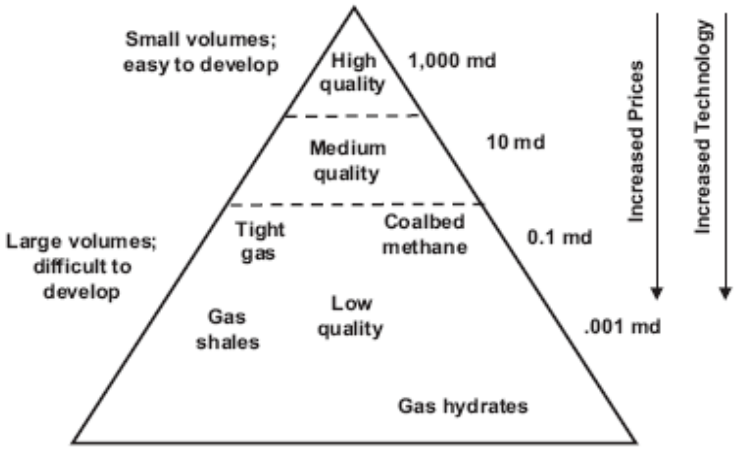

Fig. 14 – A comparison of low quality fluids and permeability[5]

Production of Tight Gas in the United States

Reported amounts of gas in place from tight gas reservoirs have constantly increased over the years which is expected as new fields are discovered and new technologies are being created to recover more fluid and to better estimate original gas in place.

The Gas Technology Institute estimates gas production throughout the year 2000 to be 58 Tcf and proven reserves to be 34 Tcf[5]. **Fig. 15** gives a visual representation of how the fluids from tight gas reservoirs are classified. The reserve class represents the amount of reserves produced that year plus proved reserves remaining in the reservoir. Recoverable reserves are those which are believed to be able to produce with existing technology but wells have yet to be drilled and field developed. The undiscovered category contains the gas that is likely to be discovered from known tight gas basins[5]. Resources are considered to be the gas in place in tight gas basins.

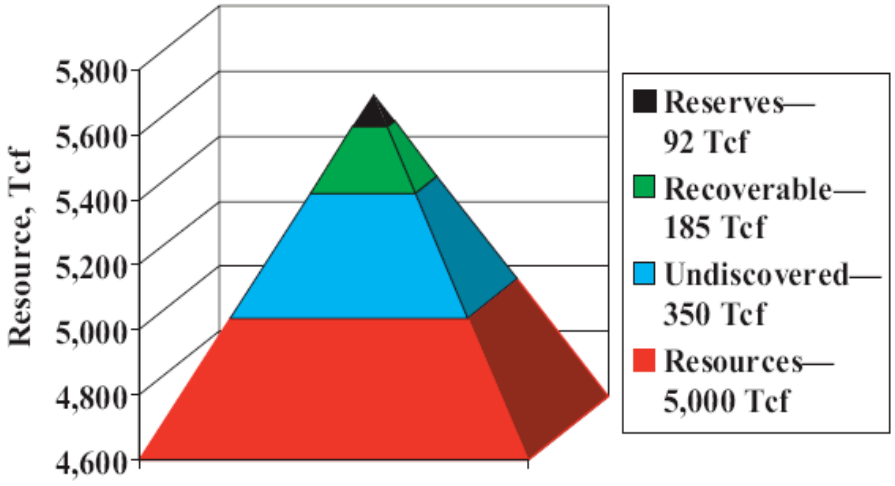

Fig. 15 – Resource pyramid for tight gas classification in the U.S.[5]

In 2004 the total gas in place from tight gas sands were estimated to have increased to 15,000 Tcf with annual production to be between 2 and 3 Tcf. At this time a reported 40, 000 wells were producing from the various reservoirs at an average production rate of 170 Mcf per day[10].

The United States has developed around 30 tight gas basins spread around the entire country, the biggest of which are the Great basin in Nevada, the Permian Basin in Texas/New Mexico, the Gulf Coast Basin, and the Appalachian Basin. These are illustrated in **Fig. 16.**

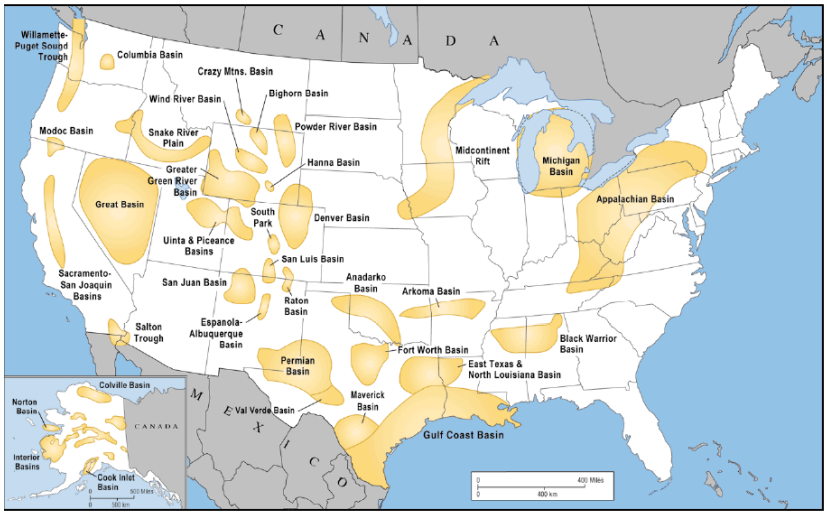

Fig. 16 – Tight gas basins in the U.S.[11]

Properties of Tight Gas Reservoirs

To return to the main purpose of this study, which is the sealing of API long thread connections in tight gas sands wells; we identify critical reservoir properties which play a part in the sealing of pipe and casing connections. By reviewing the various drilling projects and data acquired in the process we can have an idea of some of the parameters we need to overcome to create leak-tight seals. This review covers tight gas sands from all over the world including several from within the United States.

Algeria

Tiguentourine Field

The Tiguentourine field is a tight gas sandstone reservoir located in the southern part of the Illizi basin of east Algeria. In 2007 the field was investigated by BP-Sonatrach-Statoil to evaluate its characteristics. Well tests, interference tests, reservoir models, and large-scale observations were done. **Table 3** shows some of the applicable reservoir properties that were found.

Table 3 – Reservoir properties of Tiguentourine Field[12]

Reservoir Temperature	230-248°F
Pressure	3263 psi
Depth	6562 ft

Ohanet Ordovician Reservoir

Bhp Billiton Algeria technical manager Chris Scott reported some of his experiences in developing a tight gas field in Algeria. The report showed that both vertical and horizontal wells were drilled. The horizontal wells were drilled under-balanced and the vertical wells were hydraulically fractured. Schematics of both well types are shown below in **Fig. 17**.

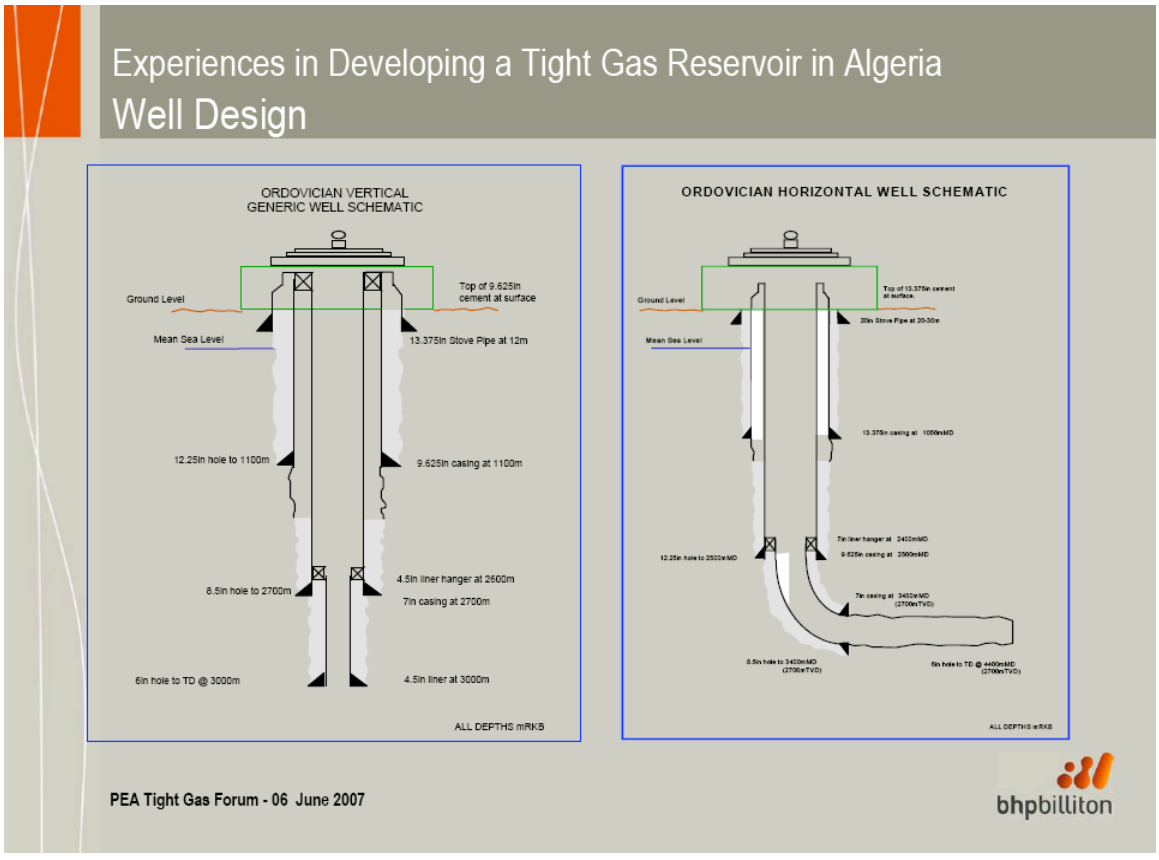

Fig. 17 – Well plan of wells drilled in the Ohanet Ordovician reservoir[13]

A more accurate report of the dimensions of the vertical and horizontal wells drilled in the Ohanet Ordovician reservoir can be seen in **Table 4** and **Table 5** respectively.

Table 4 – Well measurement of an Ohanet Ordovician vertical well

Vertical Well Measurements				
Depth (ft)	Hole size (in.)	Casing size (in.)	Liner Hanger (in.)	Liner (in.)
3609	12.25	9.625		
8530	8.5	7	4.5	
8858	6			
9843				4.5

Table 5 – Well measurement of an Ohanet Ordovician horizontal well

Horizontal Well Measurements				
Measured Depth (ft)	Hole size (in.)	Casing size (in.)	Liner Hanger (in.)	Liner (in.)
3445		13.375		
7874			7	
8202	12.25	9.625		
11155	8.5	7		4.5
14436	6			

Germany

Söhlingen Field

Gijtenbeek et al. gave a presentation on deep horizontal wells in Germany. One of the fields they studied was the Söhlingen field in Germany. The Söhlingen field has a reservoir depth of 4800m/15,744 ft, reservoir pressure of 600 bars/ 8702 psi, and reservoir temperature of 142 ^{0}C / 288 ^{0}F[14]. In 1993 a drilling project, which involved fracturing horizontal wells, was undertaken by several companies in the Söhlingen

field. The horizontal wells had 600m horizontal sections and were completed with 7 inch casing. This was reviewed and the horizontal section was now drilled with a 6-inch hole and completed with a 4.5-inch liner.

Mexico

Arcabuz-Culebra Field

The Arcabuz-Culebra field is located in the Burgos Basin in Mexico. It is a low permeability tight sand reservoir, thus requires advanced engineering in the form of hydraulic fracturing, effective well-spacing and optimum well placement for economic development.

Wolhart et al (2000) discussed how Pemex Exploration and Production (PEMEX) utilized the services of Pinnacle Technologies (tiltmeter fracture mapping, fracture and reservoir engineering), Geomechanics International (geomechanics studies), and Branagan and Associates (microseismic fracture mapping) to develop this field by combining their specialties.

From seismic and production data it was deduced that the field is compartmentalized. The target producing reservoirs were established as Wilcox 4, Wilcox 3, Wilcox 2 and Wilcox 1 sands. Wilcox 4 is a clean reservoir of high porosity and low permeability gas sands that requires hydraulic fracture stimulation. Wilcox 2, 3 and 4 sandstones have target zones located occurring at depths of roughly 7,875 ft to 8,700 ft[15].

When conducting the tiltmeter fracture mapping the Wilcox 4 sands was found to have a reservoir pressure of 4,100 psi and high downhole temperatures of (250°F-270°F).

Colorado

Piceance Basin 1

The Piceance basin is located in Garfield County in the northwest section of Colorado. It occupies approximately 6,000 square miles. Two formations were highlighted. The Wasatch formation, which occurs as shallow as 3,500 ft, and the Williams Fork formation present from 4,000 to deeper than 9,000 ft[16]. The Williams Fork formation is the main producer of gas in the Piceance basin.

A range of values for the well plan gives a conductor casing of 16 to 20 inches down to a depth of 20 to 50 feet. Surface casing measures 9 5/8 inches and is placed inside the conductor casing and goes down to a depth to 500 to 2000 feet. A 4.5 or 5-inch production casing is used at the bottom of the borehole. This design is illustrated in **Fig. 18.**

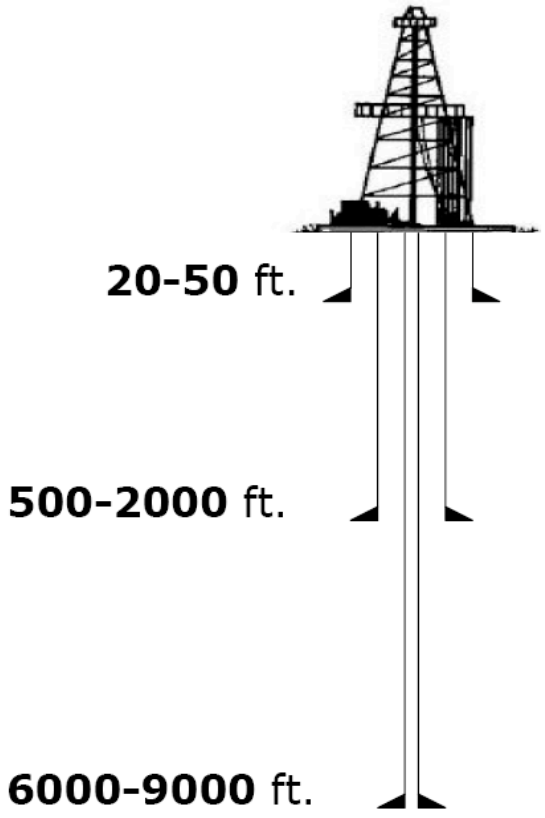

Fig. 18 – Well measurements of a well in the Piceance Basin[16]

Piceance Basin 2

A presentation made by Western Gas Resources at the Producers and Processors Technology Transfer Workshop describes their work done at the Piceance Basin as mainly focused around green completion. Green completion, as described during the presentation, is technology used to recover gas that is otherwise vented or flared during the completion phase of a natural gas well. Williams utilizes a flowback separator skid leased from Breco for its green completion operations.

Using mechanical isolation as the method of completion, the company drilled wells to depths of 6,500 ft to 9,000 ft in a low permeability carbonate sandstone formation. The Williams Fork formation has a porosity of 10% and permeability in the range of 1 to 10 microdarcies. Flow pressures ranged from 1,500 to 2,500 psi[17].

Wattenberg Field-Denver Basin1

The Wattenberg Field was reported to be discovered by Amoco in 1970. It is reported to occupy 647,272 acres of the 44,726,000 acres of the Denver Basin. It has average properties of porosity, thickness and permeability of 9.5%, 25 ft and 0.003 millidarcies. It has a formation pressure of 2750 psia. The main producing zone of the Wattenberg field is the J formation/sandstone which has a depth range of 6800 to 9300 feet**.**

Wattenberg Field-Denver Basin2

A paper written by Weimer et al. describes the Wattenberg field to the north of Denver, across the axis of the Denver basin. It has an area of 600,000 acres and estimated to have 1.3 trillion cubic feet of gas. It is classified as a tight J (muddy) sandstone with porosity ranges from 8-12% and permeability of 0.05 - .005 milli darcies and goes down to depths of 7,600 to 8,400 ft. Reservoir pressure and temperature quoted as being 2,900 psig and 260°F[18].

To drill a well in the J sandstone the well plan will begin with a 12 1/4 inch surface hole, and an 8 5/8 inch casing through the Fox Hills aquifer. Next, a 7 7/8 inch hole drilled to total depth. Following this the well will be logged and a 4 1/2 inch casing run to total depth[18].

East Texas

Trawick Field

Holditch et al. (1991) shown that tight gas formations have very low permeability thus making it challenging to produce hydrocarbons from them. To enable the engineers to predict the production from wells in tight gas the distribution of the properties throughout the formation must be known. The author set about to determine how properties, mainly permeability, vary by reviewing literature and analyzing data from the Travis Peak formation in east Texas. These activities should provide a reasonable prediction of how permeability varies from layer to layer and then can be used to predict the permeability for an average well in a formation**.**

During the review of literature a number of ways were found that would explain and sometimes predict the distribution of properties. The resource triangle explained that the higher quality hydrocarbons were easily reached but not found in abundance. The poorer quality minerals were plentiful and harder to produce. They cost more to recover.

Other literature claims a lognormal distribution can be used to predict the distributions of many formation properties. It also shows data acquired from several fields to follow lognormal distributions.

By observing data obtained from the Travis Peak formation and using probability methods to account for non-economic wells it was reported that 1.84 Bcf could be produced from a 160-acre area being drained by 100 wells. Reservoir data from the Travis Peak formation is displayed in **Table 6.**

Table 6 – Reservoir properties of the Travis Peak formations[19]

Average Depth	8000 ft
Reservoir Pressure	4000 psi
Reservoir Temperature	225 ^{0}F
Minimum Flowing Bottomhole Pressure	1000 psi

James Reservoir

Meeks et al. conducted a study in the Trawick field mainly on a redevelopment project in the James Reservoir. The James, found to be an upward shoaling carbonate reservoir, has a facies of mudstone to wackestone with intercrystalline micro-porosity. During the redevelopment an initial reservoir pressure was found to be 4,050 psi. Two pilot wells were drilled to test whether fracturing was necessary or even possible. The wells were horizontal wells with laterals around 4000 feet and production casing set at 60^0 in the build section. **Fig. 19** below gives a visual aid of the well design.

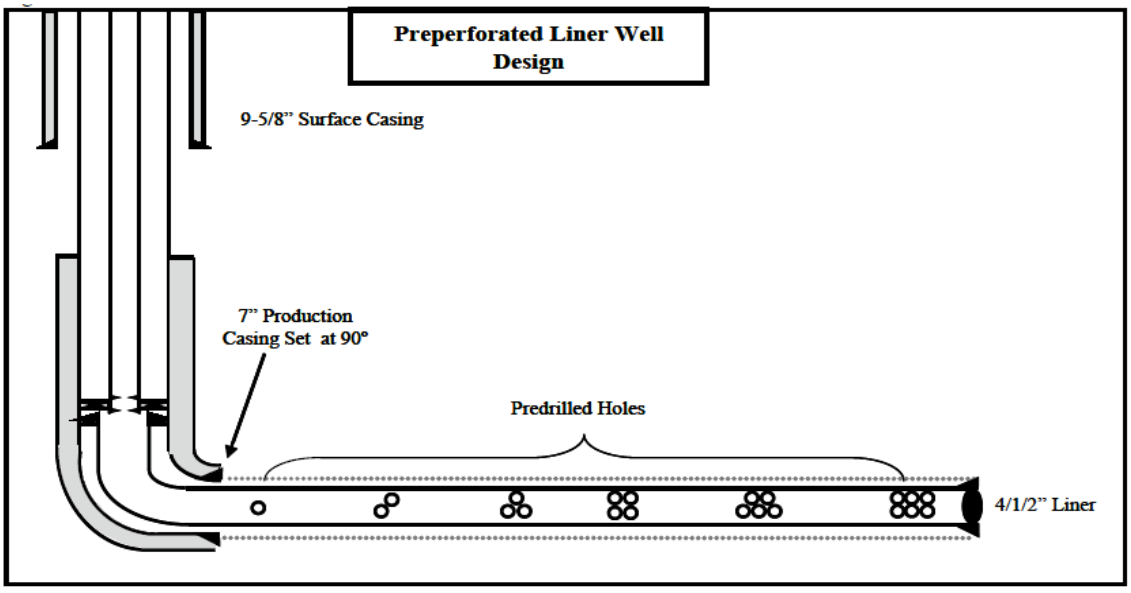

Fig. 19 – Measurements of a well in the James Reservoir[20]

Carthage Field

McCoy et al. (1996) discusses the application of horizontal drilling technology to Pirkle #2 a well in the Lower Petit formation found in the Carthage Field located in Panola County, Texas. Horizontal drilling technology is being applied to economically produce gas that was deemed uneconomic in the past. Producing at 60 MCFD was deemed uneconomic compared to 34 MMCFD produced by about 199 wells just to show how much was produced from this formation[21].

Pirkle #2 had to overcome problems such as low reservoir pressure of 210 psia, water disposal zones at 2,600 ft 2,900 ft, and 5,200 ft., and a low pressured gas pay zone above target zone may cause differential pipe sticking during drilling[21]. After overcome the negative factors of drilling certain factors were taken into consideration for the design:

- sufficient reservoir volume
- competent rock
- effectiveness of simulation on formation
- homogeneity of rock
- good vertical permeability
- medium range permeability
- large pore throat sizes
- absence of faulting and good surface well control[21]

For the drilling process Pirkle #2 was drilled with the traditional fresh water based mud for the straight hole section and the build section (90^0). The lateral was left open hole and casing set at the end of curve. After considering different systems for the lateral section the team decided on using air drilling.

The well plan begins with a 13 ½ in. hole to 2,000 ft connected to a 10 ¾ in. surface casing. A new hole size of 9 7/8 was drilled to 5,428 ft. The well would then be logged and a BHA would be attached to drill the curve section 10^0 per 100 ft. The curve section will end at 6,000 ft. TVD and a 7 in. casing set. A 6 ¼ in. will be drilled for the lateral section out to 2,000 ft with the possibility to extend.

The actual well drilled differed slightly from the well plan, but had the same general format. The hole size and casing sizes remained the same but the depths changed. The surface casing was set at 1,985 ft. MD and the build section started at 5,436 ft. The build rate was 10.34^0 per 100 feet, thus the end of curve can be found at 6,252 ft MD (5,984 ft TVD) with a build angle of about 84^0. Only a 1,432 ft. of lateral was possible after many problems were encountered. After the well was completed and started producing the flowing pressure was measured to be 143 psig. A summary of all values are compiled in **Table 7** and a diagram of the well profile is shown in **Fig. 20.**

Table 7 – Completion design for a Carthage Field well[21]

Well Plan		
Measured Depth (ft)	Hole size (in.)	Casing size (in.)
0-2000	13.5	10.75
2000-5428	9.875	
5428-6000	9.875	7
6000-6000	6.25	
Actual Well Design		
Measured Depth (m)	Hole size (in.)	Casing size (in.)
0-1985	13.5	10.75
1985-5436	9.875	
5436-5984	9.875	7
5984-6015	3.5	

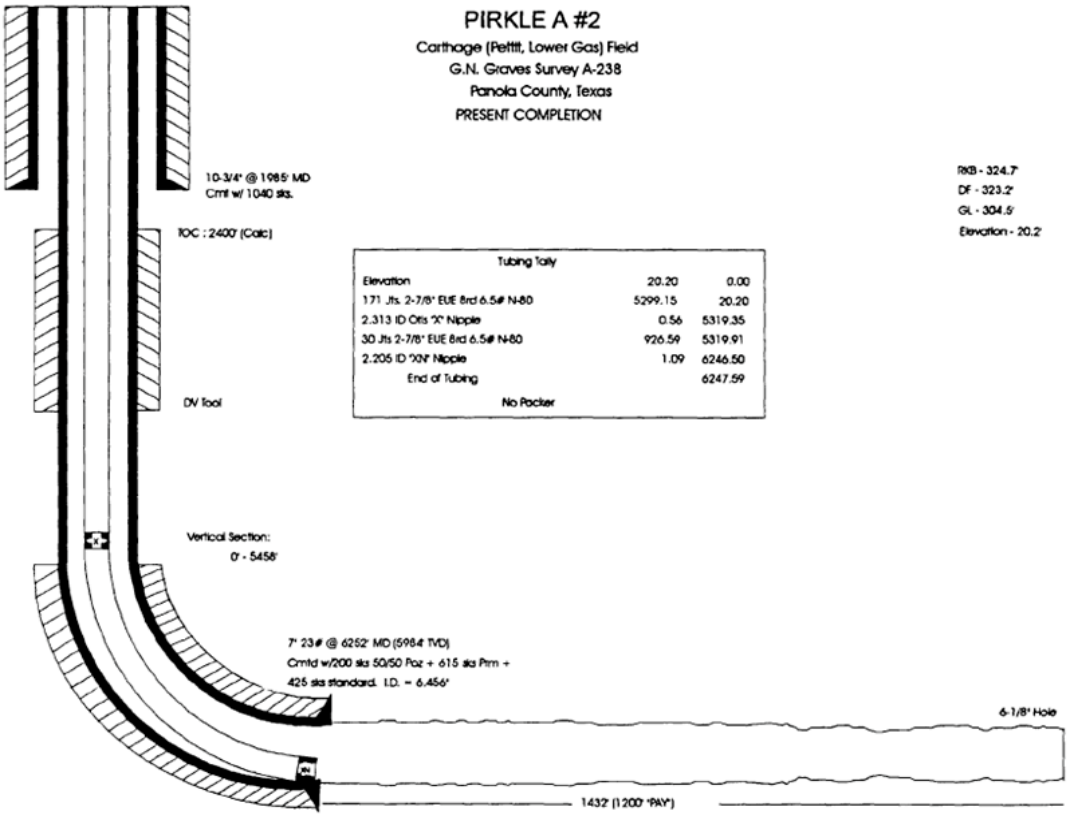

Fig. 20 – Completion design for a well in Pirkle #2[21]

Data Analysis

After combining all data obtained for the various tight gas fields all values were tabulated in **Table 8.** The midpoint of the data ranges was used to quote an average parameter for the field. This table was used to create the following graphs, which show a comparison of the various fields.

Table 8 – A collection of all reservoir properties reported

Location	Reservoir Temperature (^{0}F)	Reservoir Pressure (psi)	Depth (feet)	Length of lateral (feet)
Algeria	239	3263	6562	3281
Egypt	298			
Germany	288	8702	15744	1698
Mexico	260	4100	8288	
Piecance Basin1			6500	
Piecance Basin2		2000	7750	
Wattenberg Field1		2750	8050	
Wattenberg Field2	260	2900	7900	
Wattenberg Field3	220	3250	8000	
Travis Peak	225	4000	8000	
James Reservoir		4050		4000
Carthage Field			6000	2000

To get a better idea of how the parameters compare across the different fields the data from each field were plotted. Beginning with reservoir pressure **Fig. 21** shows a bar graph of the reservoir pressures reported from the different fields. The abbreviations PB, WB, and JR represent Piecance Basin, Wattenberg Field, and James Reservoir respectively. Fields in Algeria, Germany, and Mexico are the other fields where reservoir pressures were reported.

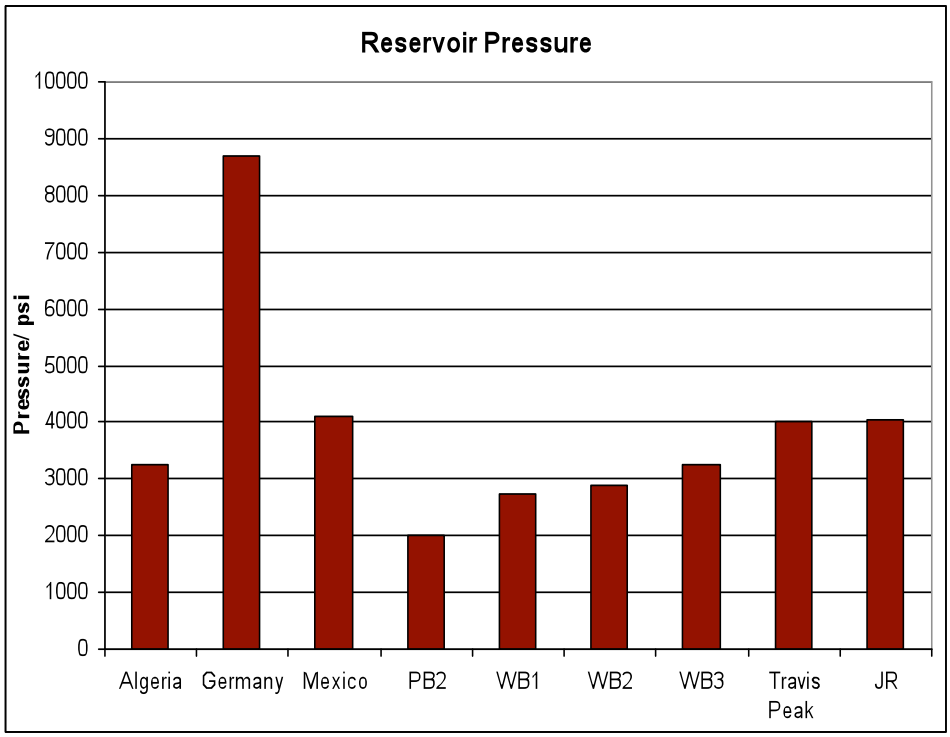

Fig. 21 – Bar chart comparing reservoir pressures

A scatter plot of the reservoir pressures reported is shown below in **Fig. 22** along with the average of all available reservoir pressures. Besides the one major outlier, the Germany field, the reservoir pressures hover around the 3500 psi mark.

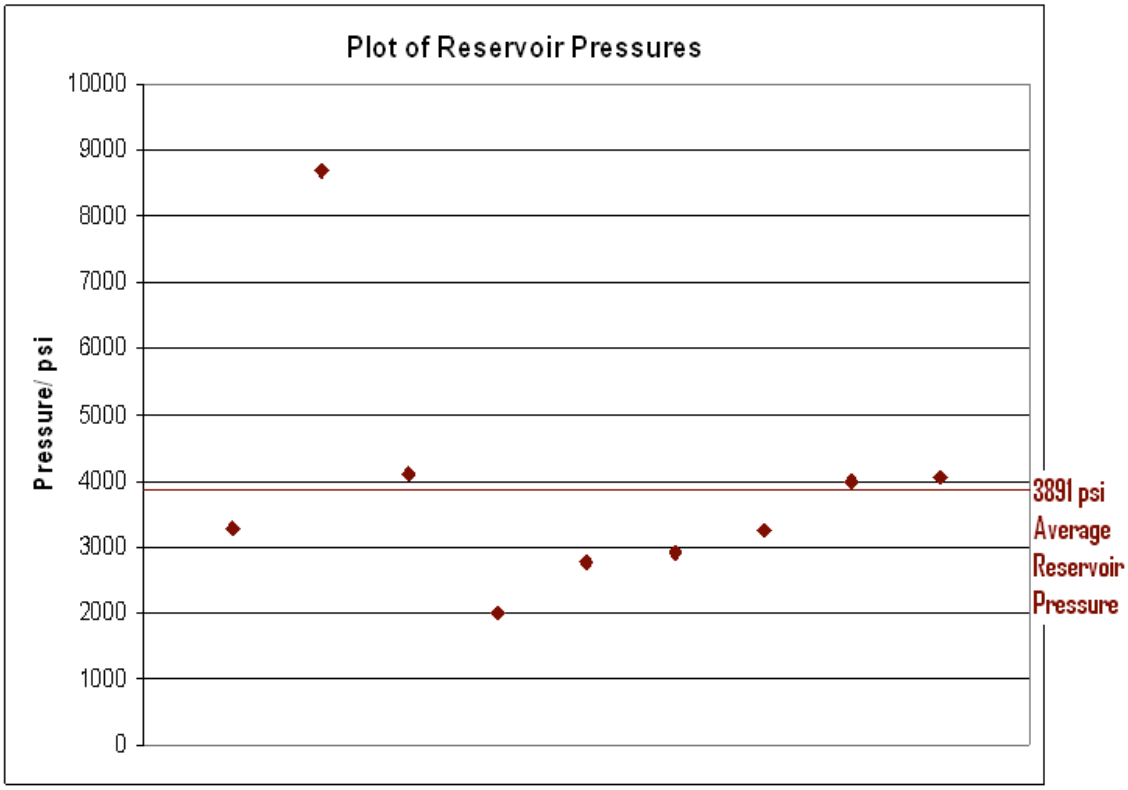

Fig. 22 – Scatter plot of reservoir pressure

Fig. 23 shows a bar chart of the reported reservoir temperatures. The fields in Algeria, Egypt, Germany, and Mexico along with the Wattenberg field and the Travis Peak formation are those with reported reservoir temperatures.

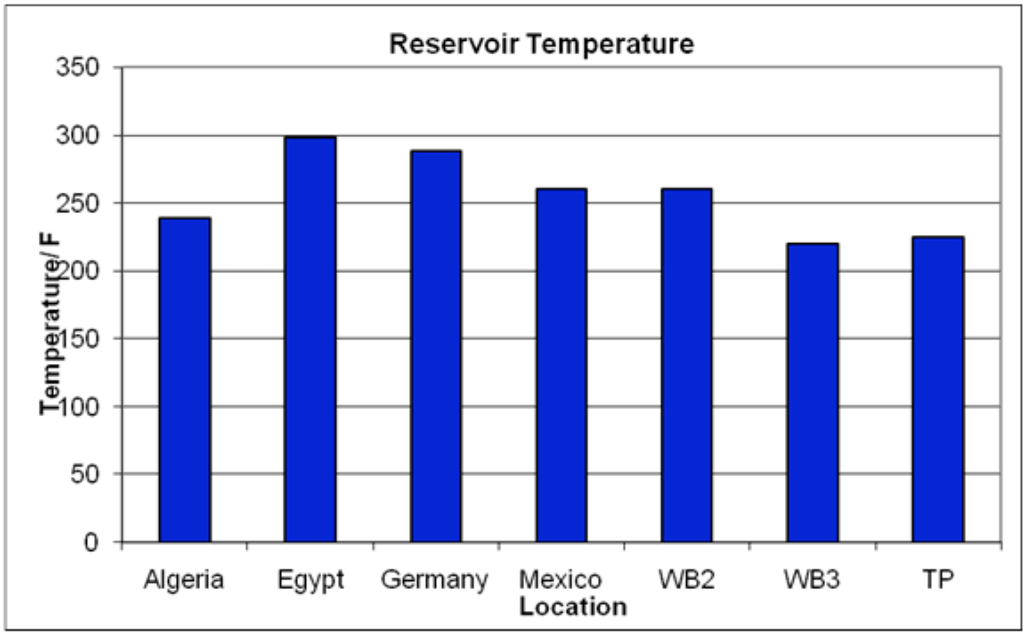

Fig. 23 – Reservoir temperatures of some tight gas fields across the world

Fig. 24 displays the reported reservoir temperatures in the form of a scatter plot, which also displays the average of all the temperatures available.

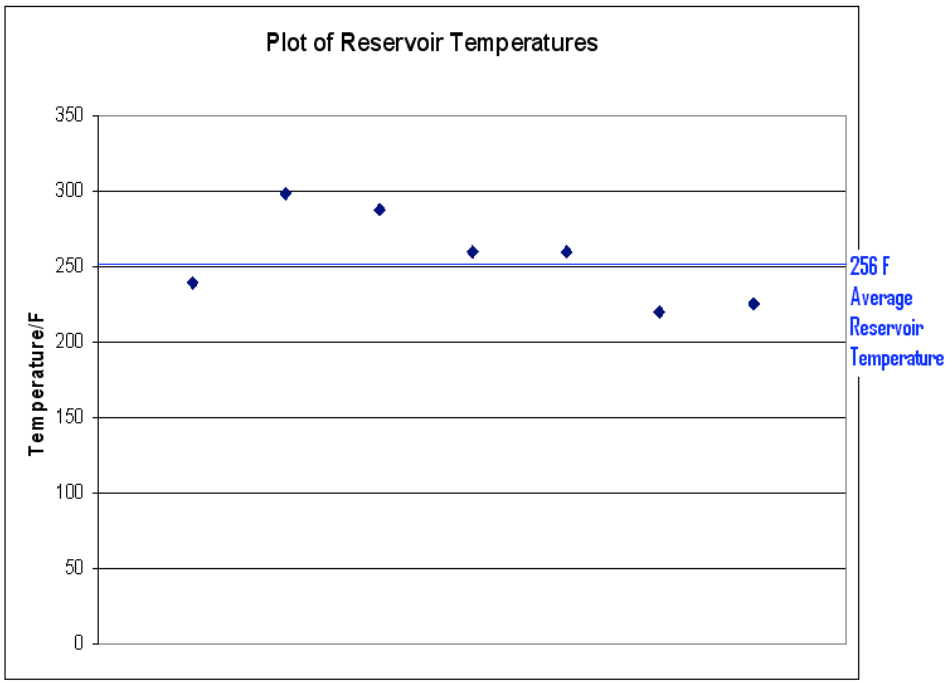

Fig. 24 – Scatter plot of reservoir temperatures

Most of the fields worldwide reported some depth of the wells drilled in the tight gas fields. They all were roughly around the 8,000 ft range with the exception of Germany, which was almost twice as deep. This compares well to the pressure plots, which showed a similar shape. **Fig. 25** displays the data of the depth of tight gas reservoirs.

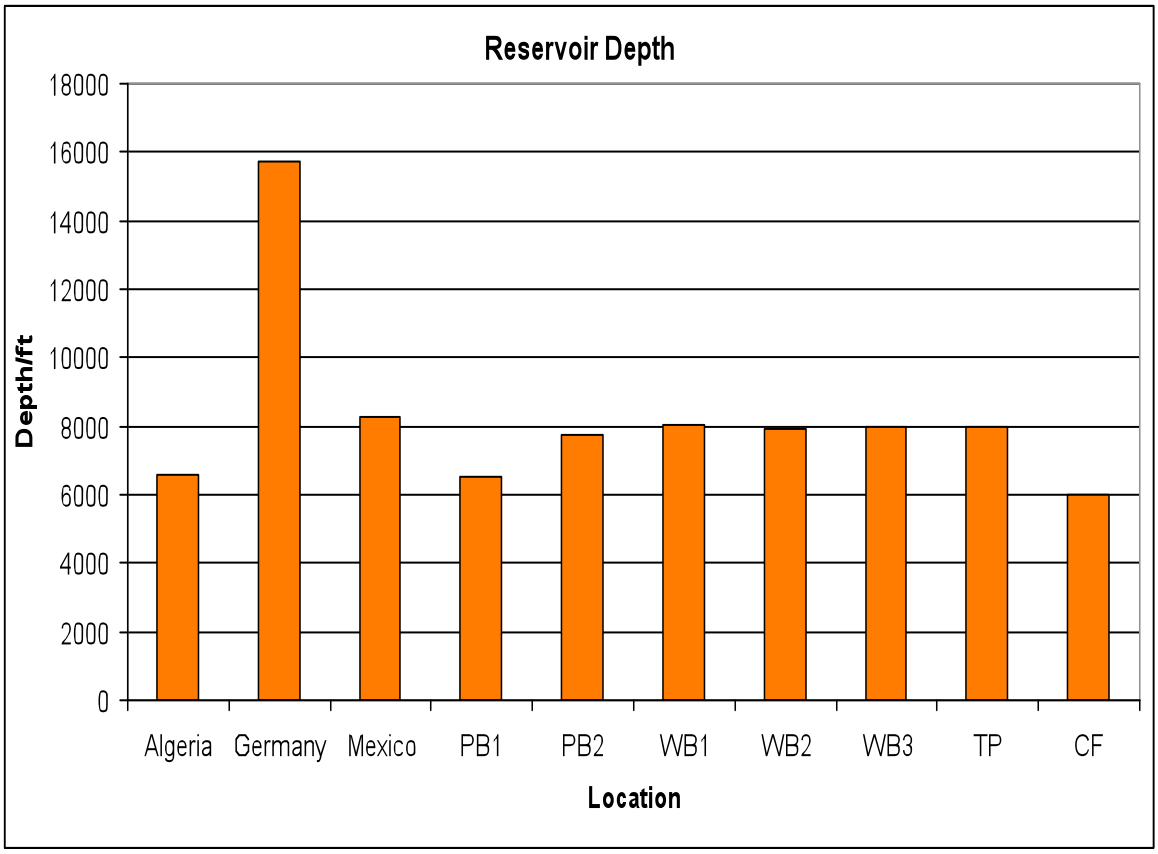

Fig. 25 – Depth of tight gas sands

Fig. 26 shows a scatter plot of the depths reported for the various fields. The mean of the depths are also displayed.

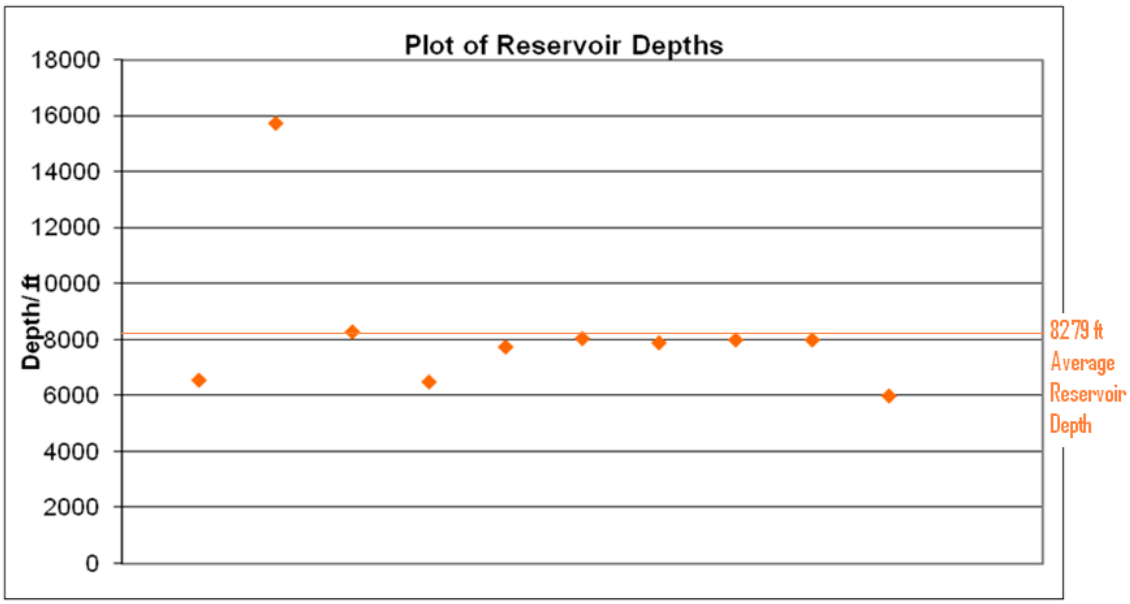

Fig. 26 – Scatter plot of reservoir depth of tight gas fields

Overview of Tight Gas Reservoir Properties

The investigations carried out for several parameters of tight gas reservoirs all around the world have shown fairly constant values. There was an indication that depth of reservoir may impact the other properties, as is the case with conventional reservoirs. A summary of the data is displaced in **Table 9.**

Table 9 – Summary of reservoir properties

	Temperature	Pressure	Depth
Average	256 ^{0}F	3891 psi	8279 ft
Minimum	225 ^{0}F	2000 psi	6500 ft
Maximum	298 ^{0}F	8702 psi	15744 ft

For the well design of wells drilled in the various gas tight reservoirs, the most common surface casing to be used was 9 5/8 in. Production zones were mainly completed with a 7 in. casing or left open-hole. However, the Pirkle #2 horizontal well design in the Carthage field had a hole size of 3.5 in. in the

production zone. 4.5 in. liners and liner hangers were used at different depths in most wells according to the formation characteristics. The surface holes varied between 12.25 in. and 13.5 in.

TESTING THE SEALABILITY OF API THREADS

Numerical and Experimental Distribution of Temperature and Stress Fields in API Round Threaded Connection

An investigation into the capability of tubing threaded connections to withstand different loading conditions such as internal pressure, tensile load, and alternate load was done. The 10-round connection performance was analyzed using finite element analysis and experimental tests. Finite element analysis was performed using Machine Readable Cataloging (MARC). Thread galling, the fusing of the pin end and the box end due to heat, is a problem involving complicated non-linear equations for stress, strain and displacement. The results of thread galling can be seen in **Fig. 27.**

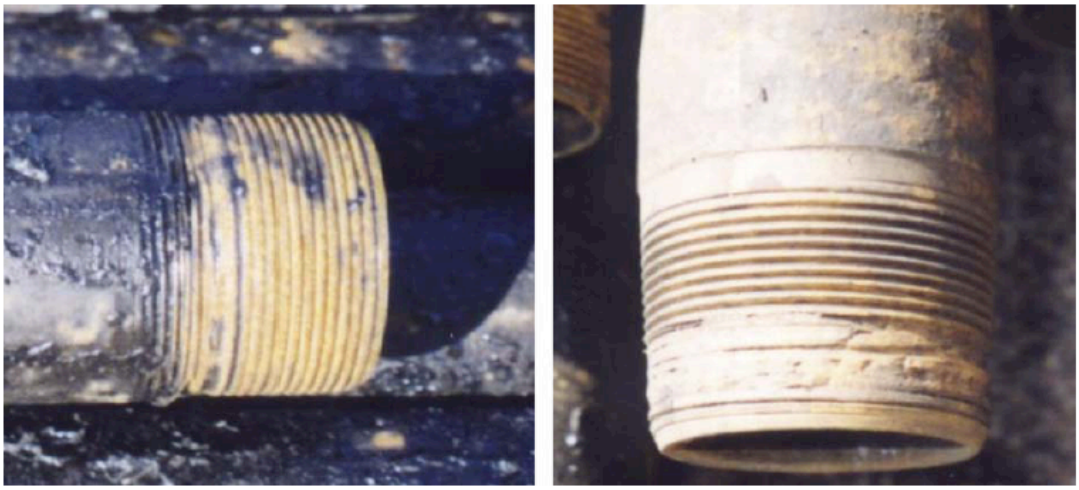

Fig. 27 – Pictures of field tubing thread showing galling[22]

Analysis of Simulation Results

The finite element analysis showed that the equivalent stress increases with the number of turns applied during make-up. The stress was highest at the ends of the connection and in the pipes. The strain measured 6,000με at the first pin of both ends of the connection.

The normal contact force was observed to be highest at the ends of the connection, which is according to observed thread galling failure, it was also noticed that the taper of the pin was affected and the pitch diameter was reduced by make-up or break-out. A tensile load, when applied to the connection, caused a decrease in the value of the normal contact force. Tension was found to reduce the sealability of an API 10-R tubing connection even though the leak resistance equation set forth by the API does not depend on tension.

Torque can be split into friction torque and deformation torque, however for API 10-R non-upset tubing connections only the friction torque is significant. It is defined by the equation[22]:

$$T_{FR} = \sum_{K} \int_{S_K} \mu \sigma_{nn} r dS_K \quad \text{.....(4)}$$

where r is the radius at the integration point; σ_{nn} is the normal contact stress; μ is the friction coefficient; S_K is the contact number K. Large friction forces occur at the ends of the threaded connection which relates to galling failure found at the end of connections in oilfield.

Experimental Study

A 73.03 × 5.51 mm J-55 API 10-round non-upset long tubing threaded connection was chosen as the test sample, where it underwent a series of make-up and break-out processes. The connection was loaded with 0.125, 0.25, 0.5, 0.625 and unloaded with 0.25, 0.3, 0.5 and 0.6 turns.

For the first step of the procedure the geometry of the sample was measured. Next, the sample was pasted on the outer surface of the pipe and the inner surface of the coupling in both the axial and circumferential directions with foil gauges. Strain and temperature readings were taken in relation to the thread.

Results of Experimental Study

The experimental study showed the sample was made and broken four times, with a significant amount of galling being evident at the fourth breakout time. The galling coincides with strain at the ends of the connection, which agrees with the finite element model. The strain value at this point exceeded 8,000με.

The make-up and breakout process produces significant friction forces and thus gives rise to thermal strain, leading to the acceleration of galling failure. The increased friction is an indication of an increase in temperature. The effect of temperature was observed using a thermal tracer showing changes during make-up and breakout. As make-up torque increased, the temperature increased to a maximum of 65 ^{0}C at the maximum torque and velocity (1,776.1 Nm and 25 rpm). This increased was first seen at the ends of the connection to validate the finite element model. Galling failure was first observed when the temperature of the coupling outer surface exceeds 55 ^{0}C.

Results from experimental work were able to verify simulation results. The main conclusion that can be taken from this paper is the confirmation that galling is major at the ends of the connection.

Investigation of API 8 Round Casing Connection Performance

In 1984 Asbill, Pattillo, and Rogers produced a series of papers describing work they carried out on API 8-round casing connections. They highlighted the distribution of stress, strain, sealability, and torque under the varying load. In the first installment the author investigated the mechanical behavior of the API long thread and coupling 8-round thread connections using finite element models (FEM) and a strain gauge test connection. This investigation fills the need for information describing how sealability is affected by the transfer of load from the stab flank to the load flank when axial tension is applied which leaves the pressure on the stab flank at a minimum, and therefore unable to seal fluid pressure.

For these experiments one of the most common casing types was used. A 7 in.-29 lb/ft sized pipe of P-110 grade using three turns makeup (10,000 psi internal pressure), and 3/4-in./ft diameter. More dimensions of the testing sample can be seen in **Table 10.**

Table 10 – API and test connection thread dimensions[23]

Dimension	API (nominal)	Pin	Box	
Taper (in. /in.)	0.0625	0.06288	0.06283	
Height (in.)	0.07125	0.07143	0.07385	before plating
Lead	1	0.9996	0.9999	after zinc plating

Hand calculations were also made using the dimensions of the sample connections, such as pipe inner radius, coupling outer radius and modulus of elasticity, to come up with values of contact pressure and hoop stress for both the pin and the box. **Table 11** shows the results of these equations.

Table 11 – Hand calculated contact pressures and stresses at the pin end, box end and centre of the connection[23]

	Contact Pressure			**Pin hoop stress**			**Box hoop stress**		
	Assembly	10,000 psi Internal Pressure	Total	Assembly	10,000 psi Internal Pressure	Total	Assembly	10,000 psi Internal Pressure	Total
Pin end	5309	5516	10825	-68206	47543	-20663	36101	37543	73644
Centre	5441	4779	10220	-59904	47543	-12361	42793	37543	80336
Box end	5341	4151	9492	-51739	47543	-4196	49388	37543	86931

Finite Element Models Solution

FEM analysis produced details about stress, strain, displacements, and forces. Two models were created using the pipe dimensioned above, along with the ANSYS computer program to analyze the characteristics of the connections. One model assumed a smooth tapered surface along the thread (no threads) to capture local discontinuity effects. The second model contained threads which made it possible to give the distribution of contact pressure at both stab and load flanks. The results obtained by Asbill et al. are as follows:

- Contact pressure is a minimum at the centre of the flank.
- Minimum assembly contact is 8,500 psi and increases to 12,500 psi with the internal pressure.
- Pressure in the root/crest clearances reduces flank contact to 5,500 psi and leakage by the flank would occur.
- High contact at the ends occurs from geometric discontinuity effects and galling should initiate at the flanks ends, particularly at the pin ends.

Strain Gage Test Connection

The sample connection mentioned above was instrumented with 24 two-element strain gauge rosettes placed along the pin inner diameter and coupling outer diameter. The sample was assembled to three turns past hand-tight (400 ft-lb). Three turns gave a torque of 5,538 ft-lb. The coupling was floated and "nongauged" end made up 2-3/4 turns. Internal pressure was measured to a limit of 10,000 psi measuring strain at 1,000 psi intervals. The weld-on end caps gave a pressure end load of 300 kip. The pressure was held for 66 hours.

The axial stress distribution for each of the models discussed above was plotted for easy comparison. **Fig. 28** shows the graph of the axial distributions.

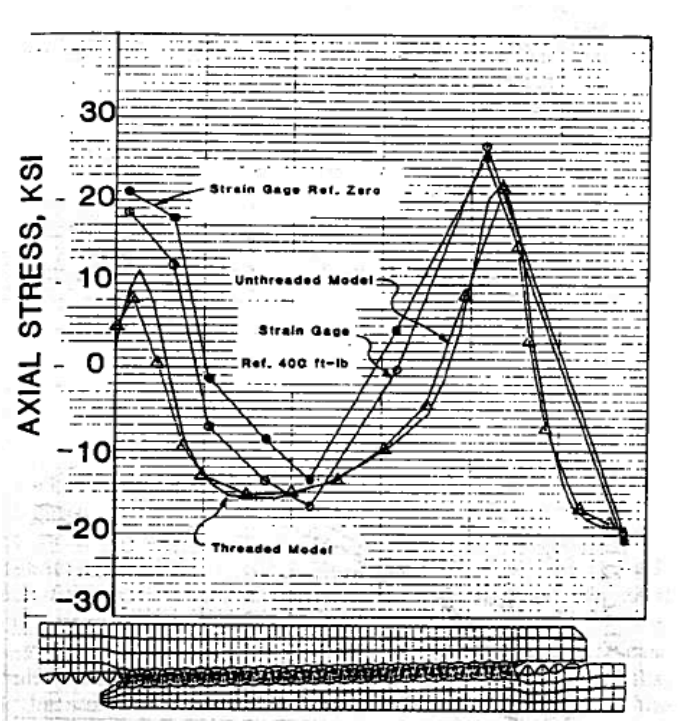

Fig. 28 – Axial stress of the threaded model, unthreaded model, and straing gauge tests at different positions of the connection[23]

Stresses and Criteria

The second installment of the series continues to investigate the effects of external loads on hoop stresses in the pin and coupling and the maximum number of turns. The extremes in the thread taper tolerances were also investigated. A slow pin/fast box refers to the tolerance levels in the construction of the connection. A slow pin is constructed with large tolerances whereas a fast box has very small thread tolerance. A slow pin/fast box fit gives maximum makeup interference at the pin end. A fast pin/slow box interference could not seal 10,000 psi. Near the middle, the predicted maximum sealing pressure was 6,048 psi[24].

The maximum number of turns was measured using two materials N-80 and P-110 on a 7 in.-29 lb/ft sized casing. For nominal pin and box taper N-80's maximum number of turns was found to be 3 turns. The P-110 had a maximum number of turns of 4.1. For the fast pin/slow box the maximum number of turns for N-80 was found to be 4.4 and P-110 5.4. At this many turns (5.4), 11,220 psi and 660 kips, the yield strength of the outer end portion of the coupling is exceeded and produces a maximum strain that is safely within the material ductility[24].

Sealability and Torque

This edition of the investigation focuses on connection sealability based on the assumption that the contact pressure in the mated surfaces must equal or exceed the fluid pressure being contained. Leak tightness is achieved by 1) the thread lubricant which provides the seal in the thread clearance and 2) the mating thread flanks, which must have a contact pressure greater than the fluid pressure.

In **Fig. 29** below the minimum contact pressure for the stab flank is shown. The pressure was the highest at the pin end decreasing to zero over the last seven threads, except for the very end. The highest value of 4,400 psi occurs at the pin end and reduces to zero seven threads away.

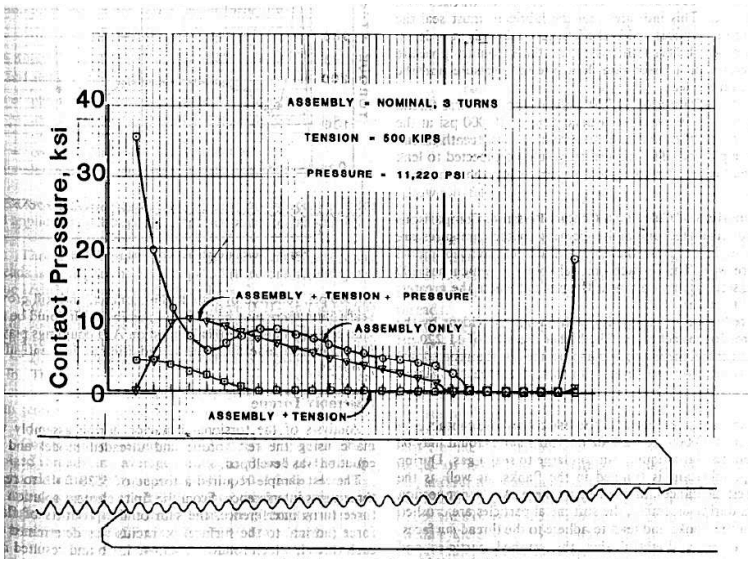

Fig. 29 – Contact pressure for assembly, assembly plus tension, and assembly plus tension plus pressure[24]

Therefore in order for the flank pressure to remain higher than the internal pressure the lubricant must seal the leak passage within the first seven threads. The clearance at the flanks that lose contact is in the order of 0.00001 and 0.00002 in. These values were minute enough to seal a liquid, but too large to seal a gas.

Assembly Torque

The test sample required a torque of 5,538 ft*lb to reach three turns interference. A coefficient of friction was calculated to be 0.021 using the **Equation 5**[25].

$$\mu = \frac{Torque}{\Sigma(F \times R)} \quad \text{..... (5)}$$

Effects of Axial Tension and Internal Pressure on Assembly Torque

It is shown by comparison that an increase in tension has little effect to torque, but an increase in pressure has a significant increase. Nominal tapers at three turns have a torque of 5,538 ft-lb. An addition of 500 kips tension increases the torque to 5628 ft-lb and the torque increased to 10,480 ft-lb when the pressure was increased by 11,220 psi. This comparison shows that for higher pressures more torque is necessary in the make-up or break-out process.

Assembly torque can also be varied by a number of variables. Surface finish, coatings, thread lubricant, and speed of makeup. The figure above shows the distribution of the torque. The ends of the connection experience the high torque values that explain galling occurring mainly at the ends. The torques values measured were 210 and 530 ft-lb. The centre of the threads has a torque of 194 ft-lb per thread. This can be seen in the graph displayed in **Fig. 30.**

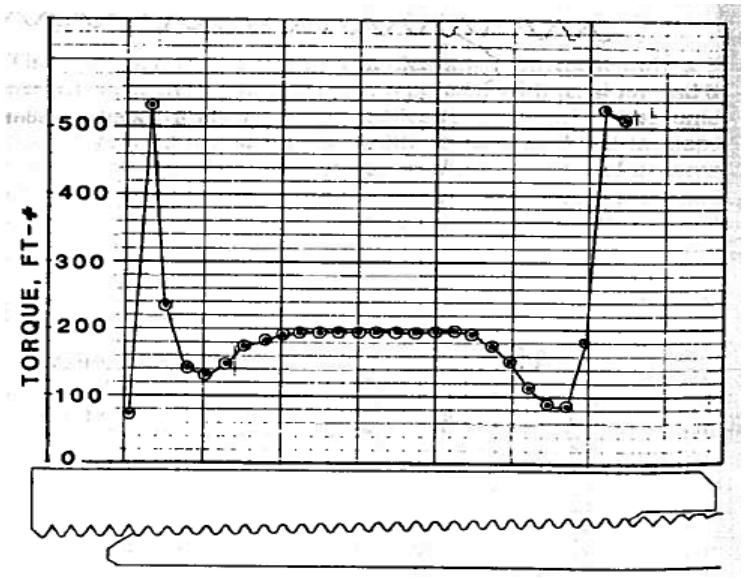

Fig. 30 – Graph showing torque values along the connection[25]

TESTING API THREAD COMPOUNDS

The Role of Thread Compounds

Thread compounds are a special type of grease used for making up drill pipe, casing and tubing. **Table 12** shows the general make-up of thread compounds percent by weight.

Table 12 – Composition of API-modified thread compound[3]

Constituent	Solids	Compound	Pass no. 325 Sieve
Grease Base	--	36	--
Amorphous Graphite	28	18	30-80
Lead Powder	47.5	30.5	30-92
Zinc Dust	19.3	12.2	90-100
Copper Flake	5.2	3.3	99-100

Thread compounds consists of base grease and contain dispersed particles and sometimes additives to improve lubrication under load conditions. Thread compounds can be classified according to toxicity: compounds containing lead, lead-free compounds, metal-free compounds and biodegradable compounds. They can also be classified according to use, whether for conventional casing and tubing strings, connections on a rig, to prevent unscrewing, or for premium connections. **Fig. 31** displays the comparisons of environmentally friendly and use of the different types of compounds.

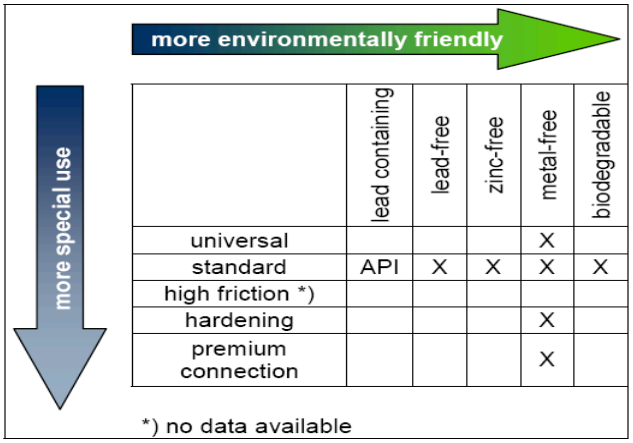

Fig. 31 – Classification of thread compounds used in tests by use and toxicity[3]

The main functions of the thread compound are to lubricate the thread during make-up to prevent galling, to seal the gap between the male and female threads to get a tight connection, and to protect the thread from corrosion. This is important to avoid leaks from appearing. A leaking tubing connection may lead to an expensive workover and to a loss of production.

Tightness Testing

Unfortunately, no simple standardized test method can test sealing performance. However, in 2006 a test method that incorporates the advantages of full scale testing and a plate method was reported. A tapered 10-round thread cut on 2- 7/8 in. tubing and sealed on the end with a welding cap was the test sample used. Using helium gas at a pressure of 200 bars (~2900 psi); the test pipes were connected to a manifold and subjected to a temperature load up to a maximum of 300 ^{0}F or 572 ^{0}C for long durations. Thread compound was applied to the threads similar to the way it was done in the field and the connection made using a hand operated torque wrench.

Fig. 32 shows the test samples all stacked in the drying cabinet on the left of the picture and connected to gauges and a gas cylinder of helium.

Fig. 32 – Picture of test apparatus showing simulated pipe connection[3]

A total of nine thread compounds, which includes two API-modified compounds were tested using this testing procedure. The compounds were run four at a time which each compound run on four different test assemblies to show consistency of results.

After running these tests, they compared the different thread compounds on the basis of pressure change during the test. The performance of the connections and thus the thread compound was compared using the pressure at the end of the test as a percentage of the initial pressure. A rating of 100% shows there was no gas leakage, but a 0% showed all the gas leaked out.

Contrary to expectations, the more environmentally friendly compounds, metal-free, lead-free, biodegradable and lead-API- modified compounds performed better than the other compound containing harmful compounds. This result was contrary to current beliefs. **Fig. 33** shows the results of all nine compounds and how well they performed.

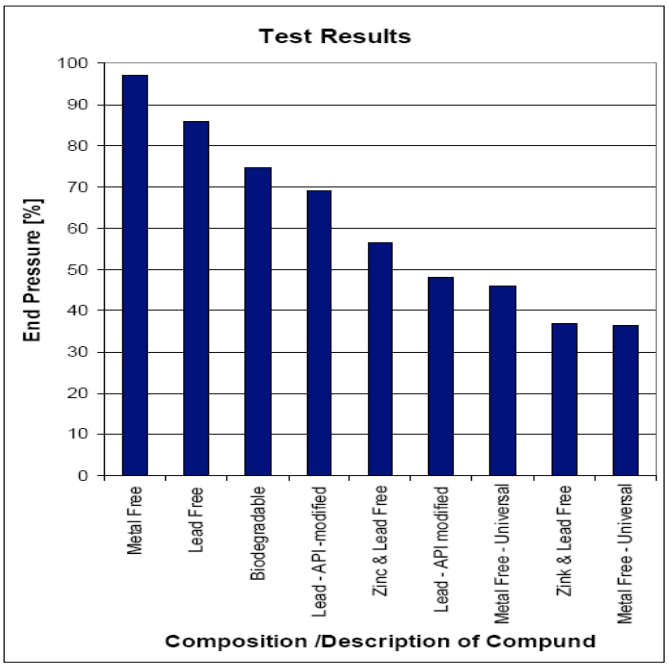

Fig. 33 – Results of the tightness tests[3]

The new sealing test method fulfils the requirements of API and ISO for a seal-tightness test for thread compounds. This method can be used to compare thread compounds under certain conditions. The tests showed that the cheaper, more environmentally friendly compounds provided better sealing characteristics.

Grooved Plate Method

In 2007 Badicioiu and Teodoriu used a grooved plate method to investigate the seal capacity of thread compounds in thread connections. The grooved plate test has a unique construction, shown in **Fig. 34,**

which enables it to isolate the performance of the thread compound from other parameters of the connection such as thread tolerances, stresses, and strains.

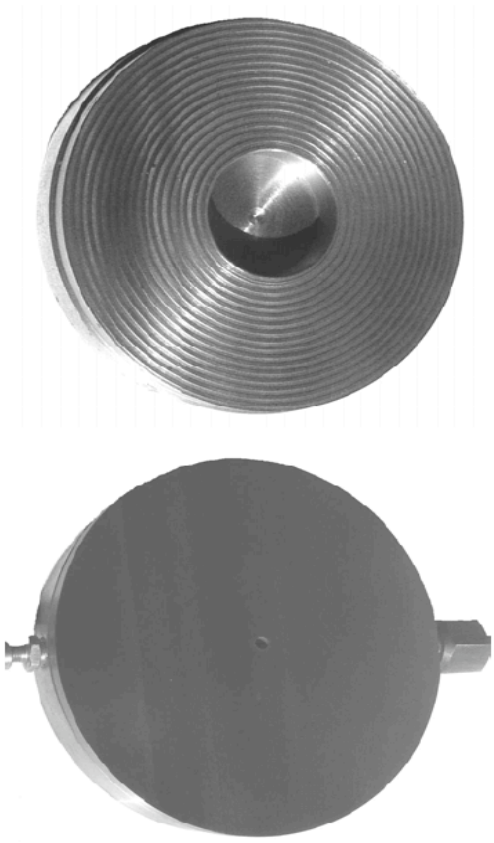

Fig. 34 – Pictures of the grooved (top) and seal (bottom) plates[1]

To carry out the experiment, the thread compound to be tested was generously applied to the grooved plate before the connection was made by clamping both plates together. The connection was then placed in a hydraulic press where a contact pressure was applied using a pressurizing medium. Mineral hydraulic oil can be used as well as nitrogen as the pressurizing medium. An initial contact pressure is applied to the connection and increased until the dope is expelled from the side of the connection.

Two propriety connections, an API Modified compound, and an API compound containing ploymers were tested and it was found that the API compound has the lowest leak resistance when used in conjunction with the API thread type. These results are displayed in **Fig. 35.**

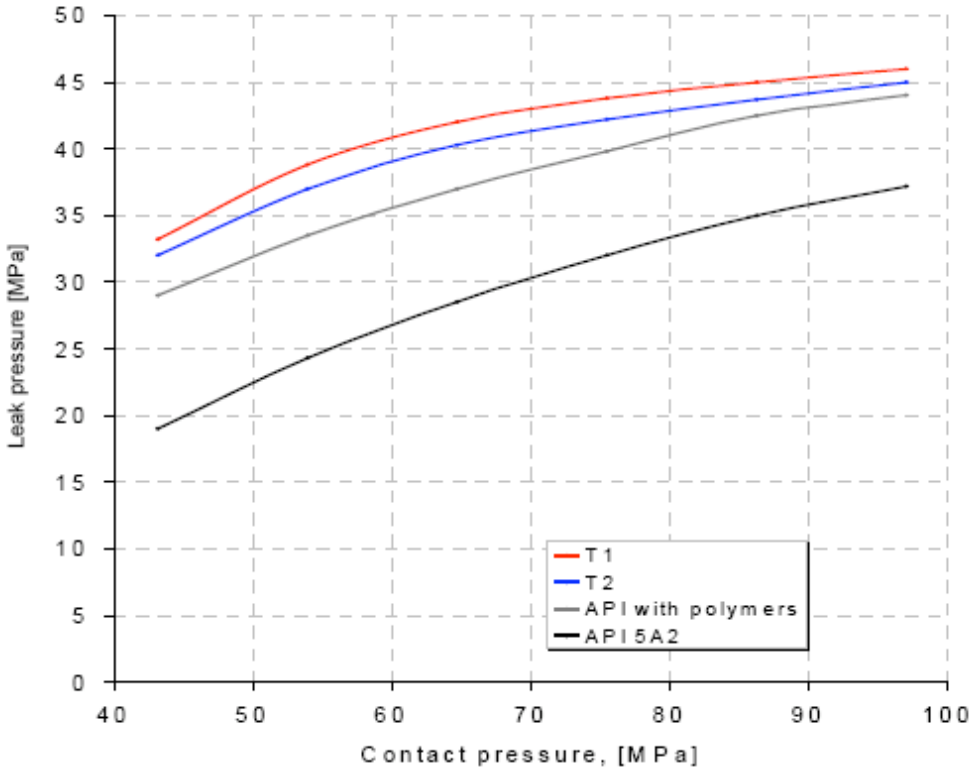

Fig. 35 – Graph showing leak pressure as a function of contact pressure[1]

Slot Flow Theory

This theory is used to describe flow through rectangular slots. It can be adapted to describe the flow of thread compound through the grooves of the top plate in the groove plate test. Slot flow theory is defined by **Eq. 6**[26]**.** By knowing the dimensions of the groove, the anticipated flow rate, and the viscosity of the thread compound we can find the pressure difference between the centre of the plate, where the gas enters, and the ends of the connection, where it is expelled.

$$q = \frac{Wh^3}{12\mu}\frac{dp_f}{dL} \quad \text{..... (6)}$$

where q is the maximum allowable leak rate measured in cubic meters per second; W and h is the width and depth of the grooves measured in m; μ is the viscosity of thread compound and measured in Pa.s; and $\frac{dp_f}{dL}$ the pressure gradient measured in Pascals.

TESTING THE VISCOSITY OF THREAD COMPOUNDS

Experiment

To measure the viscosity of the available thread compound samples, the Brookfield DV-III Ultra programmable rheometer was used. It was designed specifically for the measurement of fluid parameters of shear stress and viscosity at given shear rates. According to the operating instructions manual[27] the viscosity drag of the test fluid against the spindle is measured by the deflection of a calibrated spring. The rotational speed of the spindle, along with its size and shape can affect the viscosity measurement. Additionally, some types of fluids are considered to be thixotropic. The viscosity of a thixotropic material decreases under constant speed over a period of time. The viscosity of thread compounds was found to follow this behavior during initial practice runs and adjustments were made to the procedure to standardize results.

Thread Compound Samples

I acquired three samples of thread compound to test their viscosity. API Modified thread compound is traditionally considered the best when it comes to sealing threaded connections. NCS-30 and Kopr-Kote both manufactured by Jet Lube Inc. are the other two available samples.

API Modified Thread Compound

The API Modified thread compound is specifically formulated for use on casing, tubing, line pipe, flow lines, subsurface production tools, tank batteries, etc[28]. Apart from its sealing purposes, API Modified thread compound protects equipment with the use of rust and oxidation inhibitors blended into grease,

compounded from custom-refined low-sulphur oil. This mixture provides various benefits to the compound such as the ability to be easily applied to the thread while at the same time adhering to the thread surfaces resisting water washout and preventing rust and corrosion. It also provides adequate lubrication that reduces friction and reduces the occurrence of galling and wear.

API Modified thread compound is rated to withstand 10,000 psi without hardening or drying and functions best in the temperature range 0 ^{0}F to 400 ^{0}F. It is composed of a grease base, powdered graphite, lead powder, zinc dust, and copper flake in the ratios 36%, 18%, 30.5%, 12.2%, and 3.3% respectively. Aluminum Stearate was used as a thickener. It has a typical specific gravity of 1.70 and a density of 14.2 lb/gal[27].

NCS-30

NCS-30's solids package is formulated to prevent excessive circumferential makeup by increasing the coefficient of friction under compressive forces[29]. This is accomplished by the increase in friction factor of the compound as the stress level increases while maintaining hydraulic joint efficiency.

NCS-30 contains carbon fibers, extreme pressure and anti-wear additives which combine to form a base grease boasting superior adhesion to wet steel surfaces, resistance to water wash off and most drilling muds[29]. It provides excellent performance on high chrome or nickel alloys, additional against seizing and wear, and is extremely effective when using high pH muds.

NCS-30 thread compound contains calcium complex which serves as a thickener. It has a specific gravity of 1.30 and a density of 10.30 lb/gal. The friction factor of the compound is 1.0; this is consistent with those of drill strings as shown in the bulletin API RP 7G. For oilfield, mining, or construction drilling the compound rating for temperature is anywhere in the range of -20 ^{0}F to 500 ^{0}F.

Kopr-Kote

Kopr-Kote is a low friction anti-seize lubricant manufactured from a combination of micro-size copper flakes and graphite, dispersed in a water-resistant grease and is fortified with anti-oxidants, plus rust and corrosion inhibitors[30]. It also contains a unique additive, a product of Jet Lube, CZ-EX, which enables Kopr-Kote to provide a level of protection no other compound can.

Kopr-Kote provides a shield against metal to metal contact, thus preventing seizure and corrosion[30]. Its ability to create a matrix between mated surfaces, such as the pin and the box of a thread connection, makes it unaffected by contraction or expansion. The thread compound has the ability to fill irregularities and imperfections and resist welding, hardening, or setting[30]. Kopr-Kote also has a low shear between particles allowing quick disassembly with minimum wrench torque. This fact makes Kopr-Kote a great option for production where quick assembling and dismantling is required.

The service rated temperature for Kopr-Kote is -65 ^{0}F to 1500 ^{0}F. It has a density of 9.2 lb/gal, a specific gravity of 1.1, and a coefficient of friction of 0.11.

Equipment

Brookfield DV-III Ultra Programmable Rheometer

The HBDV-III Ultra model of this machine was used. It boasts the largest spring torque calibration which, when combined with spindle CP-52 gives a maximum viscosity of 7,864,000 cP. It is also equipped with an electronic gap setting which simplifies the procedure to set the 0.0005 inch gap between the sample cup and spindle cone. The procedure is as follows:

- The electronic toggle switch is flicked in the on position (the red light is illuminated)
- The yellow light is observed whether it is illuminated or not

- If it is illuminated the micrometer adjustment ring is turned clockwise or to the left until the light is just breaking contact
- When this point is reached the micrometer adjustment ring is turned one more division to establish that 0.0005 inches gap
- If the yellow light is not illuminated the micrometer adjustment ring is turned counter clockwise or to the right until the light is just breaking contact
- When this point is reached the micrometer adjustment ring is turned back one division to the left or clockwise to establish that 0.0005 inches gap
- After the gap is set, the toggle switch is returned to the off position before any measurements are made.

This model is equipped with a four line digital display controlled with a 20 key control pad. The information that can be read from the display is shown in **Table 13** along with their units, range of measurement, and the form of their output. **Fig. 36** shows a photo of the Brookfield Rheometer as it would be seen while making a viscosity measurement.

Table 13 – Display information of Brookfield Rheometer[27]

Item	Units	Format	Range	Example
Speed	RPM	X.XX XX.X XXX.X	0.01 <= RPM <= 0.99 0.1 <= RPM <= 99.9 100 <= RPM <= 250	0.99 2.4 150.0
Spindle		XX	00 <= S <= 99	52
Viscosity	cP	X.XX XXX.X XXXXX XXXeX	0 <= cP <= 9.99 10 <= cP <= 999.9 1000 <= cP <= 99999 100000 <= cP <= 51200000000	3.16 123.8 12345 123e3 to 8
Shear Stress	D/cm^2	X.XX XXX.X XXXXX XXXeX	0 <= D/cm^2 <= 9.99 10 <= D/cm^2 <= 999.9 1000 <= D/cm^2 <= 99999 100000 <= D/cm^2 <= 999999	4.56 234.5 12345 123e3
Shear Rate	1/SEC	X.XXX XX.X XXXXX	0 <= 1/SEC <= 9.999 10 <= 1/SEC <= 99.9 100 <= 1/SEC <= 99999	1.234 20.7 200
Temperature	^0F		-148 <= F <= 572	-10.3

Fig. 36 – Brookfield DV-III Ultra

Brookfield Refrigerated Temperature Bath

This piece of equipment is used to provide variable temperature to the rheometer. It has a digital display, fine and coarse temperature controls, hi/low safety level dial, and drain valve. **Fig. 37** shows a photo of the temperature bath.

Fig. 37 – Brookfield Refrigerated Temperature Bath[31]

Thermolyne Furnace 30400

This piece of equipment is used to heat quantities of for a long duration. It has an 864 in^{32} chamber with four heating elements capable of heating to a maximum of 1200 ^{0}C (2192 ^{0}F). The chamber also has vent ports for removal of unwanted contaminants and moistures. The Thermolyne furnace has a simple digital display showing actual temperature and set temperature. The operator has at his disposal a mechanical Over Temperature Relay, one of the safety features. Another safety feature is the door safety switch protector which is responsible for cutting off power to the elements when the door is opened. **Fig. 38** displays a photo of the furnace.

Fig. 38 – Thermolyne Furnace 30400[32]

Procedure

To measure the viscosity of thread compound a basic procedure was followed. This procedure is a combination of the procedure set forth by the standard ASTM D 2196 and that described by the Brookfield operating manual for the Brookfield DV-III Ultra programmable rheometer. This simple procedure was then combined with different loads such as temperature and time to provide an idea of the viscosity of thread compound under different conditions.

To provide a viscosity measurement over a wide range of temperatures, the rheometer was hooked up to a water bath capable of providing a wide range of temperatures.

Basic Procedure

1. The power switch was turned on to power up the rheometer
2. The rheometer was zeroed to display 0% torque
3. After the zeroing of the rheometer the cone spindle no.52 was attached to the coupling nut
4. The sample cup was placed in position under the cone spindle
5. The gap was set according to the procedure described above
6. The sample was cup was removed and a 0.05 ml sample was measured and placed in the centre of the cup
7. The cup was then replaced
8. A pre-determined spindle speed or RPM was punched on the keypad and entered
9. The motor was then turned on to begin measurement
10. The sample was left for a pre-determined time before a reading can be taken as long as the torque was above 10%

To measure the viscosity of my samples I decided to use a range of temperature between 32^0 F and 140 ^{0}F. This range was chosen due to a combination of safety and being able to measure all three samples with the same conditions. I chose an RPM of 2 for all my measurements. This RPM seemed to be the best fit for all three samples that would allow a torque reading above 10% for my temperature range. Two minutes was chosen as the length of time to be elapsed before a reading can be taken.

This procedure with its associated pre-determined conditions will then be combined with a fatigue test designed to apply cycles of varying heat to observe the change in viscosity. It is also combined with a constant temperature test where it is placed in a furnace for two weeks.

Fatigue Tests

For the fatigue test API Modified thread compound was used as the test sample. An initial viscosity measurement was read using the basic procedure at 68 ^{0}F. After the reading is taken the temperature is increased to 176 ^{0}F then returned to 68 ^{0}F where the viscosity is recorded again. This process is considered to be one cycle and is repeated 15 times in an effort to determine what kind of effect cyclic loading of temperature can have on the viscosity of the sample.

Constant Temperature Tests

The effect of constant temperature over a long period of time is the desired information to be obtained from this experiment. A significant sample of API Modified thread compound was placed in a beaker and placed in the Thermolyne Furnace for approximately 2 weeks. Viscosity measurements using the basic procedure discussed above were taken of 0.5 ml samples from the beaker at the beginning of the 2 weeks, at the end of 1 week, and on the completion of the 2 weeks. All measurements were done at 140 ^{0}F.

RESULTS AND ANALYSIS

Viscosity Measurements

API Modified

Table 14 shows the results obtained from carrying out the basic procedure for testing the viscosity of API Modified thread compound. Measurements were done three times and arithmetic mean found to give an average value. The Brookfield Rheometer also measures other parameters while taking viscosity measurements. The shear stress and torque are the other quantities measured by the rheometer along with the viscosity, while temperature is varied.

Table 14 – Results of viscosity measurements

Temperature (^{o}F)			
T_1	T_2	T_3	T_{avg}
32.9	32.9	32.9	32.9
50.36	50.36	50.36	50.4
67.8	68	68	67.9
85.8	85.8	85.8	85.8
103.8	104	104	103.9
121.5	121.6	121.5	121.5
139.4	139.6	139.4	139.5
Shear Stress (Dyne/cm^2)			
SS_1	SS_2	SS_3	SSavg
11,256	11,383	11,652	11,430
7,049	7,620	7,096	7,255
5,826	5,747	5,636	5,736
4,699	4,778	4,477	4,651
4,128	4,302	4,207	4,212
3,667	3,874	3,794	3,778
2,985	3,191	3,048	3,075
Torque (%)			
Tor_1	Tor_2	Tor_3	Tor_{avg}
71	72	73	72
45	48	44	46
37	36	36	36
29	30	29	29
26	27	26	26
24	24	23	24
19	20	19	19
Viscosity (cP)			
$Visc._1$	$Visc._2$	$Visc._3$	$Visc._{avg}$
281,000	285,000	291,000	285,667
176,000	190,000	179,000	181,667
146,000	143,000	141,000	143,333
118,000	119,000	112,000	116,333
104,000	108,000	106,000	106,000
92,473	96,839	95,251	94,854
74,217	79,773	76,201	76,730

Table 15 isolates the average values to give a more accurate view of the changes occurred in the various parameters as temperature changes.

Table 15 – Average readings from rheometer

Temperature	Shear Stress	Torque	Viscosity
32.9	11,430	72	285,667
50.4	7,255	46	181,667
67.9	5,736	36	143,333
85.8	4,651	29	116,333
103.9	4,212	26	106,000
121.5	3,778	24	94,854
139.5	3,075	19	76,730

Fig. 39 shows a graph of the relationship between viscosity and temperature. The graph shows a decline in viscosity as temperature increases.

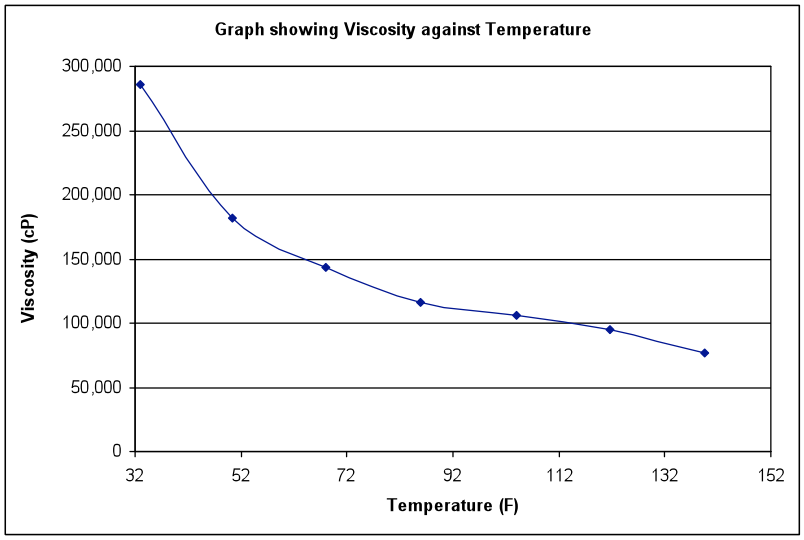

Fig. 39 – Graphical representation of viscosity measurements

An exponential curve was fitted to the data and forecasted out to 256 ^{0}F, the average reservoir temperature of the tight gas reservoirs reviewed above**. Fig. 40** displays the forecast and the viscosity value corresponding to 256 ^{0}F.

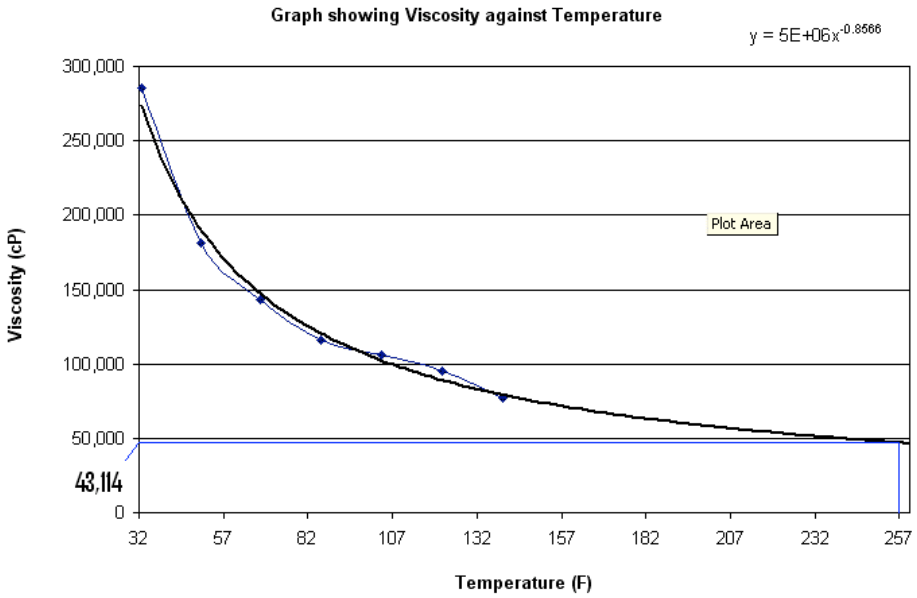

Fig. 40 – Forecasted viscosity data

Fig. 41 is a graph made from the shear stress data. The graph is made to display viscosity as function of shear stress. The graph shows a linear relationship with viscosity increases as shear stress increases.

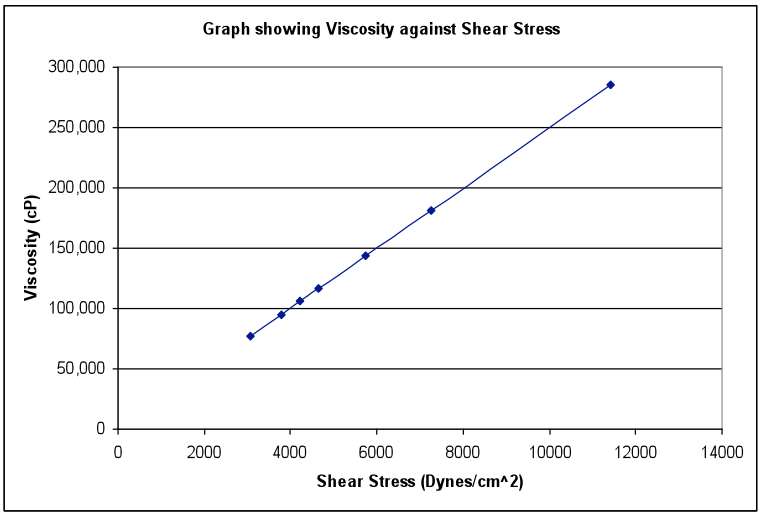

Fig. 41 – Graph displaying viscosity as a function of shear stress

Fig. 42 displays a graph showing viscosity as a function of torque. This graph is similar in shape to that of **Fig 41**. They both have a linear relationship where viscosity increases as torque increases. This is expected

because viscosity is measured by torque on the spring which is directly caused from the viscosity drag of the spindle cone on the sample material which is essentially the shear stress. Similar graphs for viscosity against shear stress and viscosity against torque validates the procedure for testing of the viscosity of thread compounds.

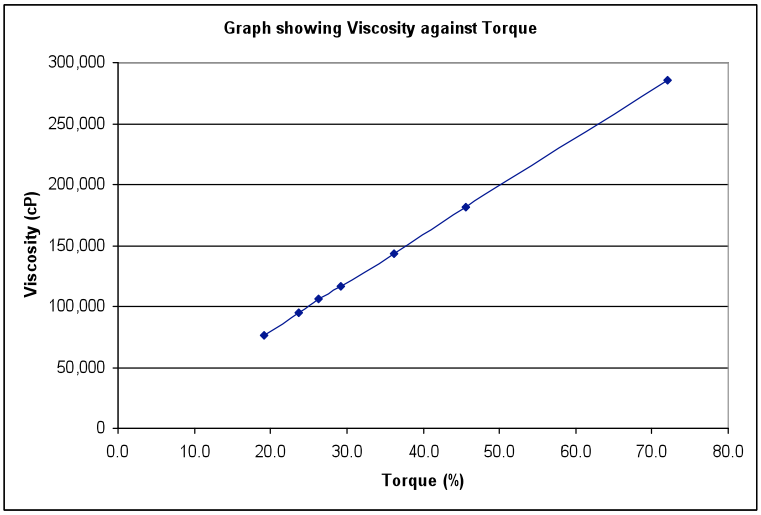

Fig. 42 – Graph showing viscosity against torque

NCS-30

Table 16 will show the data measured for the NCS-30 thread compound.

Table 16 – Measurements from the experiments performed on NCS-30

Temperature (^{o}F)			
T_1	T_2	T_3	T_{avg}
32.9	32.9	32.7	32.8
50.2	50.4	50.2	50.3
68	68	68	68.0
86.2	86	86.2	86.1
104.2	104	104.2	104.1
121.6	121.8	121.8	121.7
139.6	139.6	139.6	139.6
Shear Stress (Dyne/cm^2)			
SS_1	SS_2	SS_3	SSavg
10,382	10,621	10,192	10,398
6,922	6,541	7,064	6,842
5,461	5,493	5,302	5,419
4,477	4,524	4,270	4,424
3,889	3,540	3,747	3,725
3,254	3,191	3,366	3,270
2,508	2,937	2,932	2,792
Torque (%)			
Tor_1	Tor_2	Tor_3	Tor_{avg}
66	67	63.5	65.5
44	41.5	44.5	43.3
35	34	34	34.3
28	28.5	28	28.2
24.5	22	23	23.2
20	20	21	20.3
16	18.5	18	17.5
Viscosity (cP)			
$Visc._1$	$Visc._2$	$Visc._3$	$Visc._{avg}$
260,000	266,000	254,000	260,000
173,000	164,000	177,000	171,333
137,000	137,000	133,000	135,667
113,000	113,000	108,000	111,333
97,236	88,901	92,870	93,002
79,703	79,376	84,535	81,205
62,707	73,423	73,423	69,851

Table 17 displays only the average values, which are isolated for clarity. These are the values that will be plotted in the graphs to follow.

Table 17 – Average values from viscosity experiments

Temperature	Shear Stress	Torque	Viscosity
32.8	10,398	65.5	260,000
50.3	6,842	43.3	171,333
68.0	5,419	34.3	135,667
86.1	4,424	28.2	111,333
104.1	3,725	23.2	93,002
121.7	3,270	20.3	81,205
139.6	2,792	17.5	69,851

Fig. 43 displays the relationship between viscosity and temperature for the NCS-30 thread compound. The viscosity starts off high and gradually decreases as temperature increases.

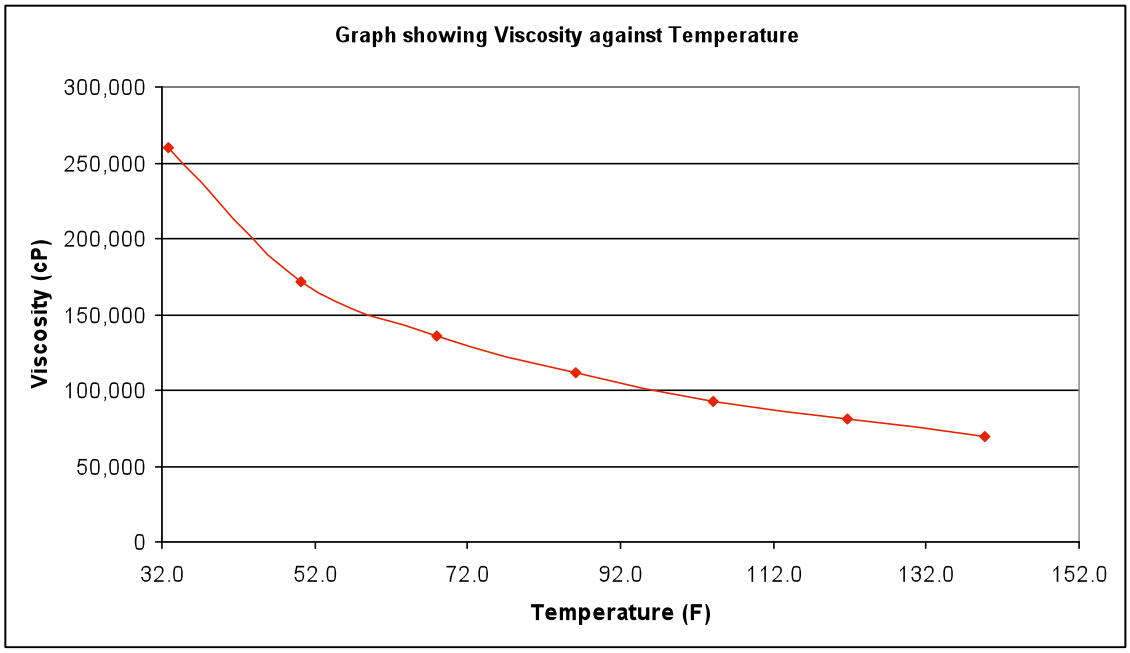

Fig. 43 – Viscosity as a function of temperature

Using the viscosity data measured a curve was fitted to the data and forecasted out to 256 ^{0}F. The viscosity value at this temperature is shown in **Fig. 44.**

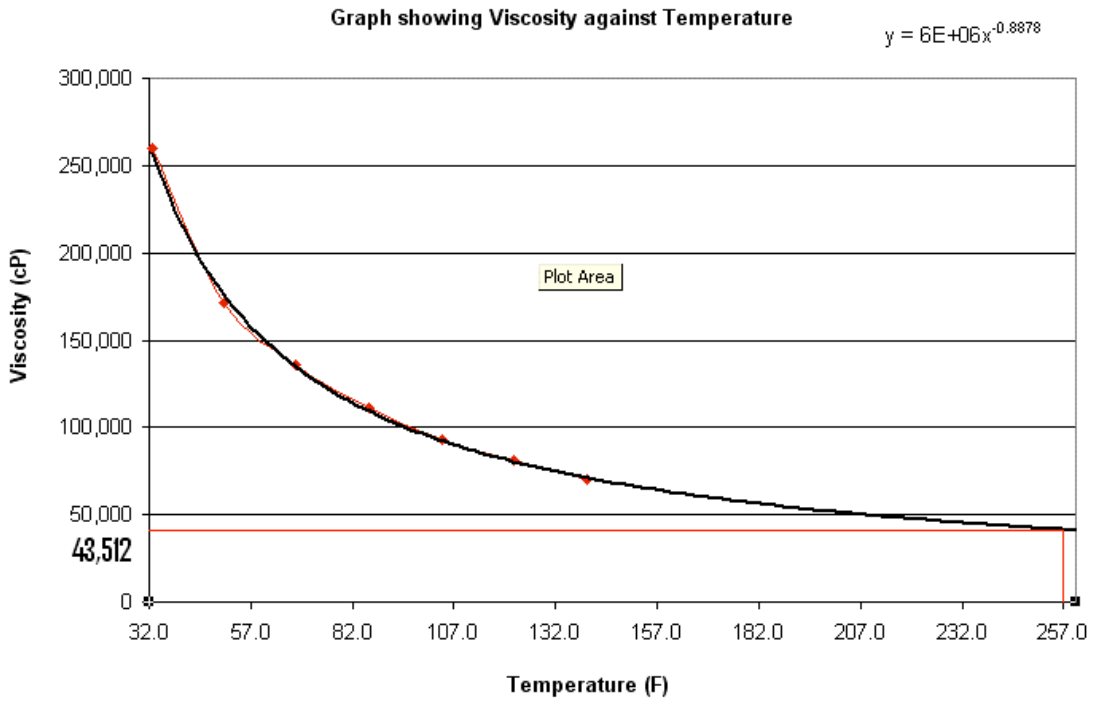

Fig. 44 – Forecast of viscosity data

Fig. 45 displays the graph of viscosity as a function of shear stress. The graph show there is a linear relationship between viscosity and shear stress. As shear stress increases the viscosity increases.

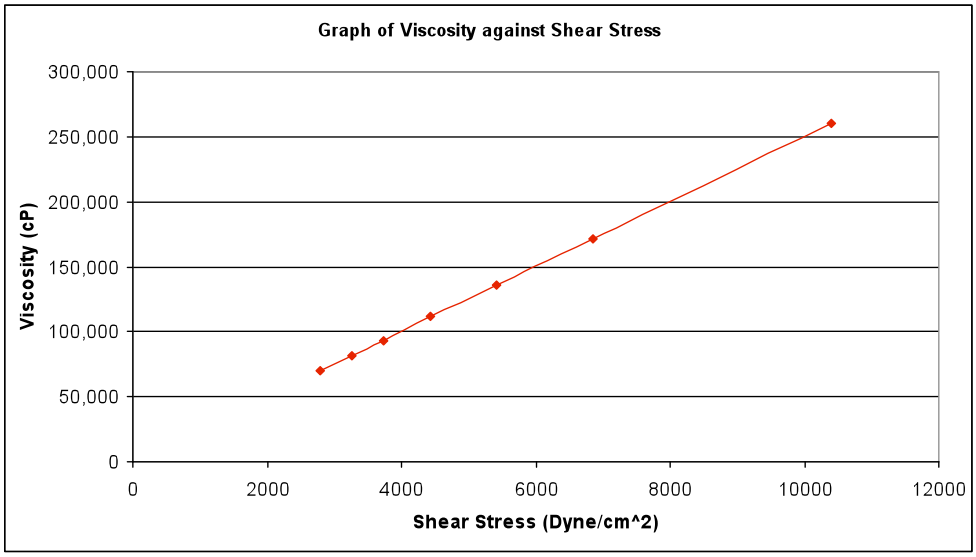

Fig. 45 – Viscosity as a function of shear stress

Fig. 46 is a graph showing viscosity as a function of torque and similar to that of shear stress torque is found to be directly proportional to viscosity.

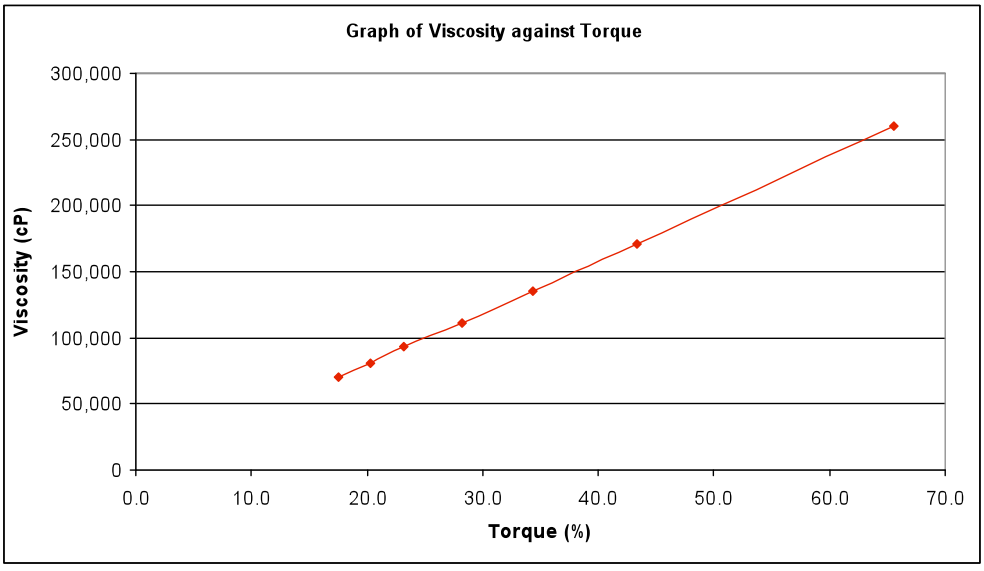

Fig. 46 – Viscosity as a function of torque

Kopr-Kote

The data collected from the experiments performed using the Brookfield Rheometer and thread compound sample Kopr-Kote is displayed in **Table 18**. It displays values of shear stress, torque, and viscosity. These parameters were read off the display unit following the basic procedure set forward earlier.

Table 18 – Results from viscosity experiments on Kopr-Kote

Temperature (^{o}F)			
T_1	T_2	T_3	T_{avg}
33	33	33	33.0
50.2	50.3	50.2	50.2
68	68	68	68.0
85.6	85.6	85.6	85.6
104	104	104	104.0
121.8	122	121.8	121.9
Shear Stress (Dyne/cm^2)			
SS_1	SS_2	SS_3	SSavg
8,096	6,683	7,255	7,345
4,461	5,334	5,223	5,006
4,143	4,096	3,858	4,032
2,905	2,873	2,963	2,914
2,175	2,143	2,175	2,164
1,857	1,857	2,000	1,905
Torque (%)			
Tor_1	Tor_2	Tor_3	Tor_{avg}
52	42	46	46.7
29	33	33	31.7
26	25	24	25.0
18	18	18	18.0
13.5	14	14	13.8
12	11.5	12	11.8
Viscosity (cP)			
$Visc._1$	$Visc._2$	$Visc._3$	$Visc._{avg}$
202,000	167,000	181,000	183,333
111,000	135,000	131,000	125,667
104,000	103,000	96,839	101,280
72,629	72,232	74,643	73,168
54,769	53,576	54,769	54,371
46,435	46,832	50,007	47,758

Table 19 shows the isolated average values of temperature, shear stress, torque, and viscosity. Its main purpose is to clearly show the trend of the values with the increase in temperature. This set of data is used to construct the following graphs showing the relationship of the parameters.

Table 19 – Average values from viscosity measurements

Temperature	Shear Stress	Torque	Viscosity
33.0	7,345	46.7	183,333
50.2	5,006	31.7	125,667
68.0	4,032	25.0	101,280
85.6	2,914	18.0	73,168
104.0	2,164	13.8	54,371
121.9	1,905	11.8	47,758

A graph displaying how viscosity changes as temperature increases can be seen in **Fig. 47.** The viscosity starts out at a high value and decreases steadily as the temperature increases.

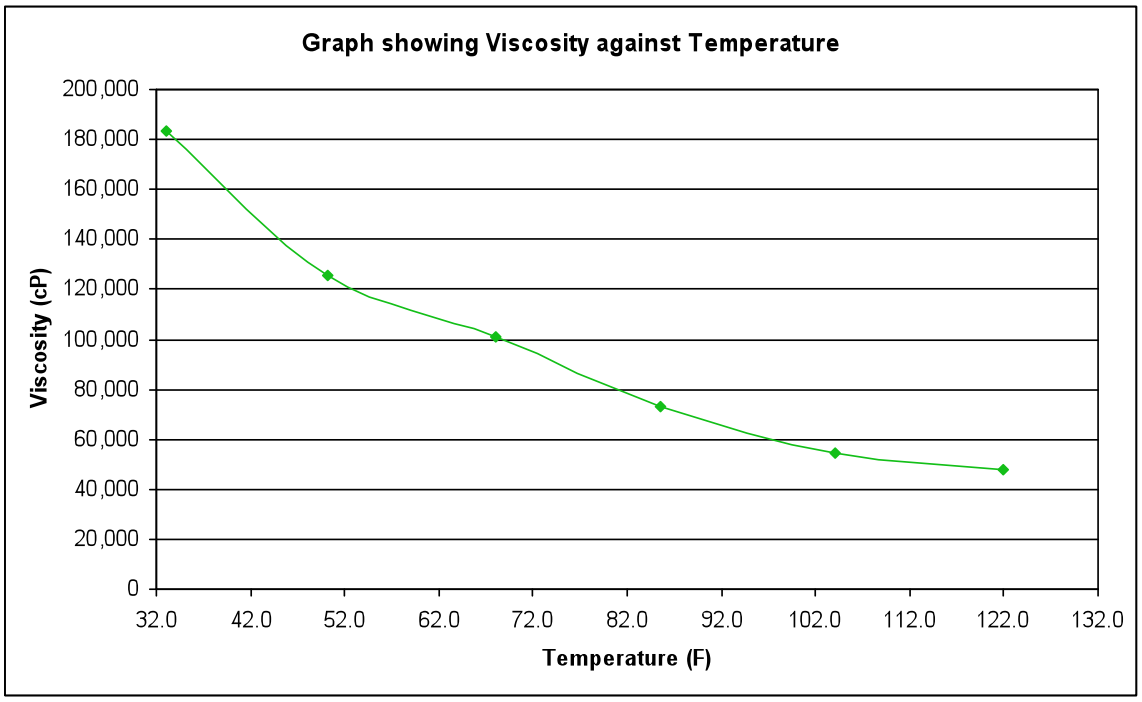

Fig. 47 – Viscosity as a function of temperature

An exponential curve was fitted to the data and forecasted out to 256 ^{0}F, the average reservoir temperature of the tight gas reservoirs reviewed above**. Fig. 48** displays the forecast and the viscosity value corresponding to 256 ^{0}F.

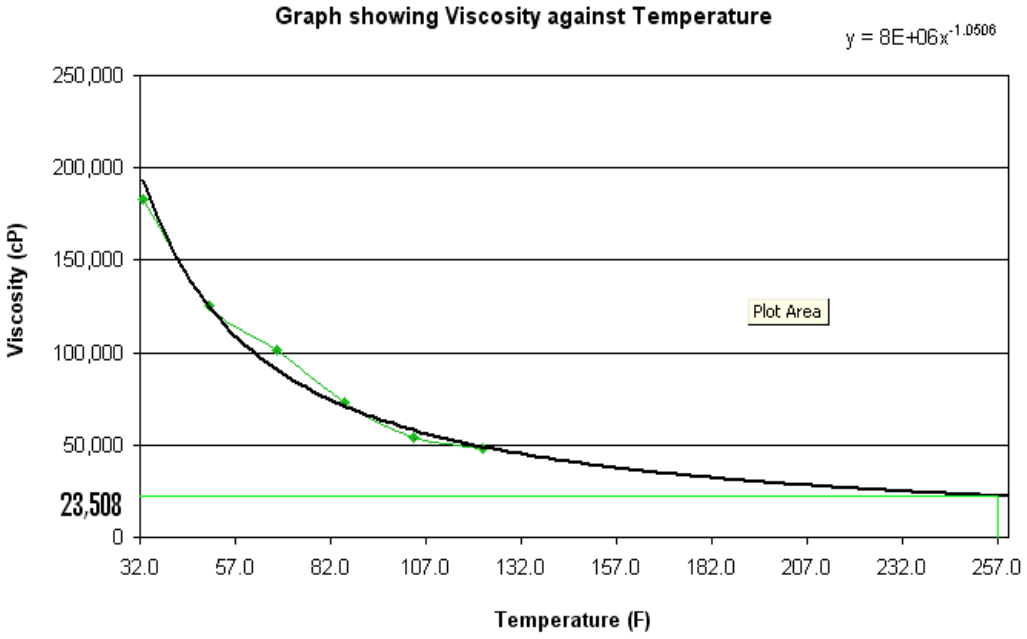

Fig. 48 –Forecast of viscosity data for Kopr-Kote

Fig. 49 displays the relationship between viscosity and shear stress. As with the previous samples a linear relationship is found.

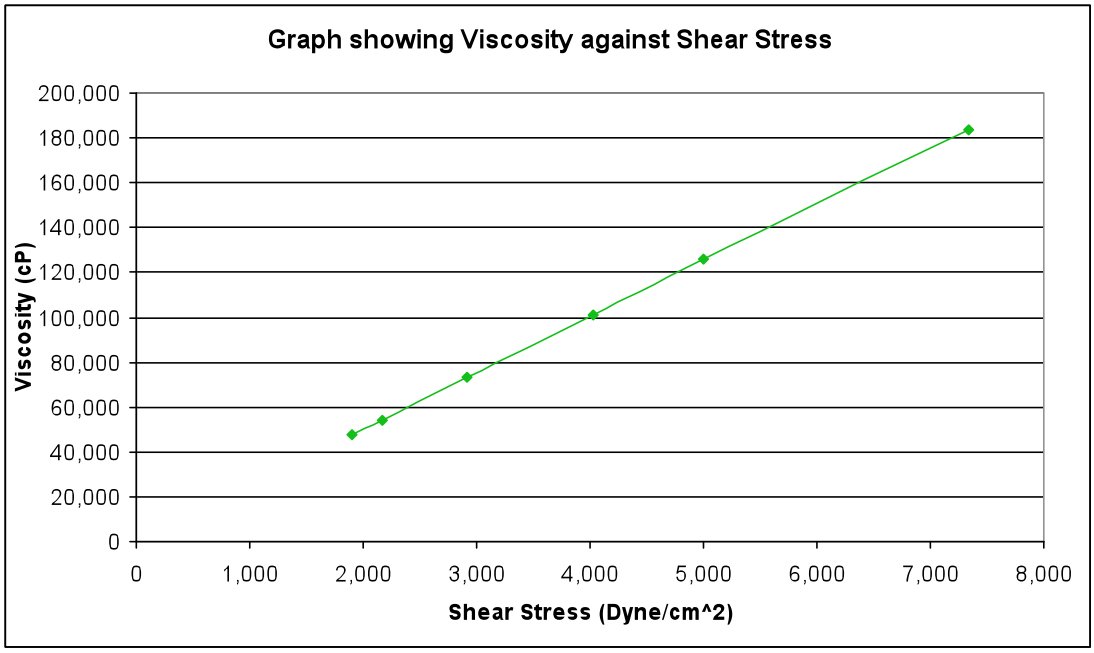

Fig. 49 – Viscosity against shear stress

Fig. 50 is the graph of viscosity as a function of torque. This is a straight line graph with a positive slope.

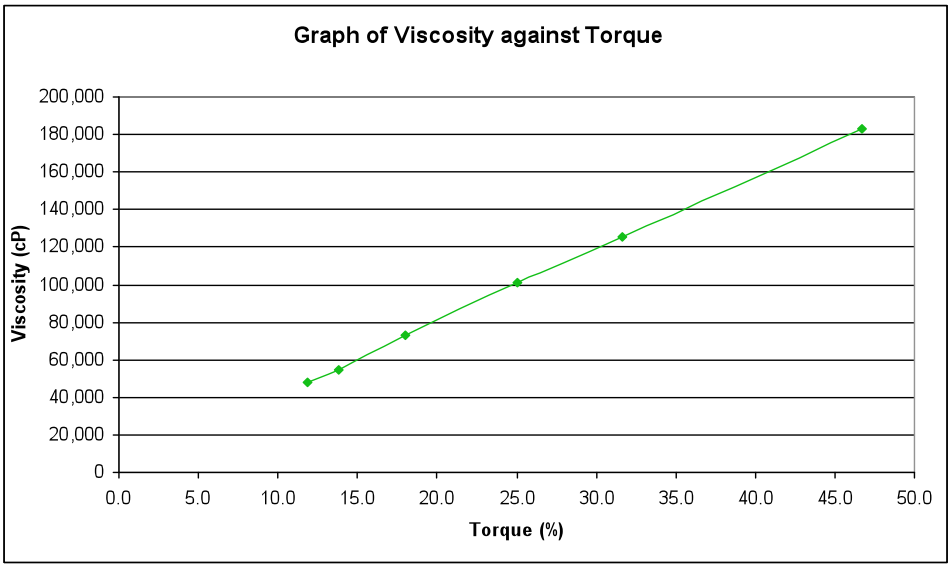

Fig. 50 –Viscosity against torque

Fatigue Tests

For the fatigue tests, only the API Modified compound was used to show its behavior under varying temperature. Over the 15 cycles of temperature loading, the viscosity of the thread compound showed a general decline in value with some fluctuation. The general decrease may be as a result of the thixotropic nature of the fluid. **Table 20** shows the data recorded from the first set of fatigue experiments.

Table 20 – First set of fatige test results

No. of cycles	Temperature (^{0}C)	Torque %	Shear Rate sec^{-1}	Shear Stress $Dyne/cm^2$	Viscosity cP
0	68	37	4	5,747	144,000
1	68.2	36	4	5,731	144,000
2	68.2	35	4	5,382	135,000
3	68	33	4	5,445	137,000
4	68.2	34	4	5,255	131,000
5	67.8	33	4	5,318	134,000
6	68	33	4	5,128	128,000
7	68	33	4	5,255	132,000
8	68	32	4	5,017	125,000
9	67.8	32	4	5,175	130,000
10	67.8	32	4	4,937	123,000
11	68.2	31	4	4,937	124,000
12	68	32	4	4,858	121,000
13	67.8	30	4	4,937	124,000
14	67.8	31	4	4,731	118,000
15	67.8	30	4	4,858	122,000

Fig. 51 shows is a graphical display of the first set of data illustrating the general decrease of the viscosity as the sample is loaded with cycles of low and high temperature.

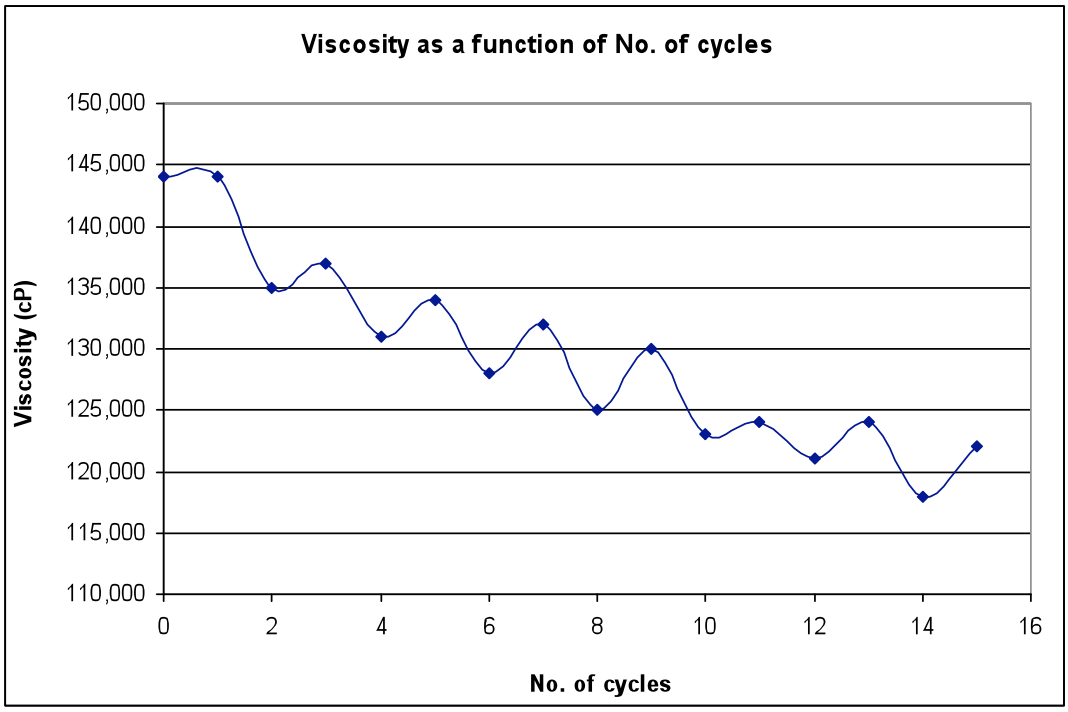

Fig. 51 – Graph showing viscosity as a function of no. of cycles

To show the results can be reproduced the experiment was repeated and produced results similar to those presented in the first set of data. **Table 21** shows the data recorded when the experiment was repeated.

Table 21 – Second set of results from fatigue tests

No. of cycles	Temperature (^{0}C)	Torque %	Shear Rate sec^{-1}	Shear Stress $Dyne/cm^2$	Viscosity cP
0	68	36	4	5,842	146,000
1	67.8	36	4	5,683	142,000
2	68	34	4	5,588	140,000
3	68	34	4	5,318	133,000
4	68	33	4	5,398	135,000
5	68	33	4	5,191	130,000
6	68	33	4	5,302	132,000
7	68	32	4	5,112	128,000
8	68	33	4	5,159	128,000
9	68	32	4	5,048	127,000
10	68	33	4	5,175	128,000
11	68	33	4	5,128	127,000
12	68.2	31	4	4,937	125,000
13	68	31	4	5,112	128,000
14	68	31	4	4,842	121,000
15	68	31	4	5,048	127,000

This data is represented graphically in **Fig.52** showing a general decrease in viscosity with more fluctuations than the first set of data but not drastically different to indicate an altogether different behavior.

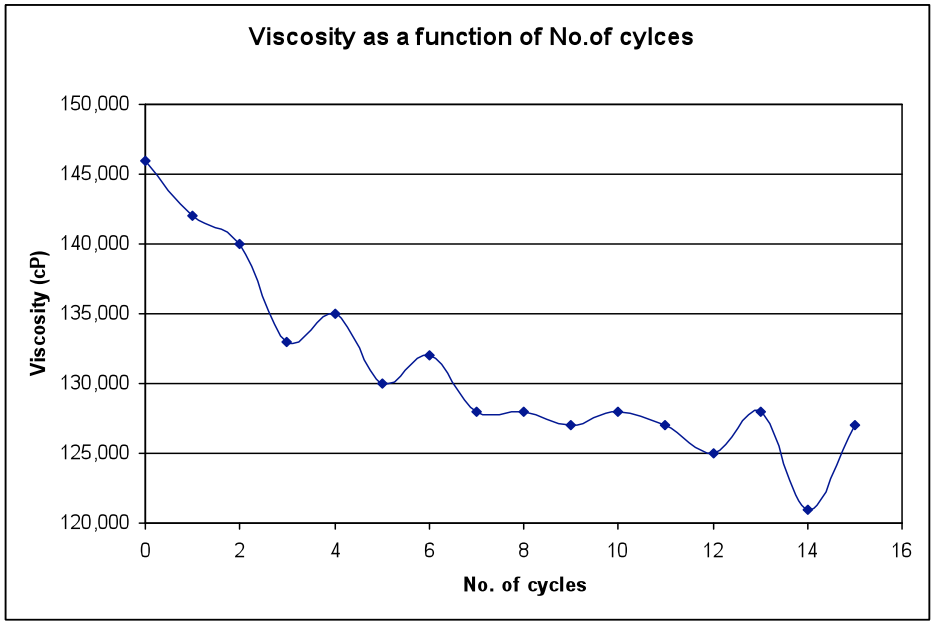

Fig. 52 – Graph showing results from the second fatigue tests

Constant Temperature Tests

The data measured from the experiments carried out after being exposed to constant heat showed that the average viscosity increased slightly after 1 week and showed a further increase after 2 weeks. **Table 22** shows the data obtained from the experiment.

Table 22 – Results from the tests with temperature held constant

	Temperature (^{o}F)			
	T_1	T_2	T_3	T_{avg}
Initial	139.6	139.6	139.6	139.6
1 week	139.3	139.3	139.3	139.3
2 week	139.3	139.3	139.3	139.3
	Shear Stress (Dyne/cm^2)			
	SS_1	SS_2	SS_3	SSavg
Initial	3,302	3,080	3,350	3,244
1 week	3,286	3,032	3,651	3,323
2 week	3,302	3,524	3,477	3,434
	Torque (%)			
	Tor_1	Tor_2	Tor_3	Tor_{avg}
Initial	20	19	21	20.0
1 week	21	19	23	21.0
2 week	21	22	22	21.7
	Viscosity (cP)			
	$Visc._1$	$Visc._2$	$Visc._3$	$Visc._{avg}$
Initial	82,551	77,392	83,742	81,228
1 week	82,551	76,201	92,076	83,609
2 week	83,345	89,695	87,314	86,785

Analysis Using Slot Flow Approximation

Using the slot flow equation and inputting dimensions of the grooves from Badiciou and Teodoriu (2007) and the maximum allowable leak rate pressure gradient were found at various temperatures for round and buttress threads. **Table 23** shows the input data held constant for the calculations.

Table 23 – Input data for slot flow approximation

	Round Thread	Buttress Thread
W / (m)	0.0007	0.0015
h / (m)	0.00008	0.0002
q / (m^3/s)	2.22E-08	2.22E-08

For calculating the pressure gradient using the slot flow equations it was found that the maximum flow rate shown in Table 22 was quoted at standard conditions, thus the flow rate was adjusted to account for the pressure conditions used during the experiment discussed by Badiciou and Teodoriu (2007). The pressure varied from 20 MPa to 70 MPa. Results for the slot flow approximation for round threads are illustrated in **Table 24**. The results for buttress threads are displayed in **Table 25**.

Table 24 – Results from the slot flow approximation for round thread

Round thread							
Viscosity (cP)	**Viscosity (Pa.s)**	**dp_f/dL (Pa)**					
		20 Mpa	30 Mpa	40 Mpa	50 Mpa	60 Mpa	70 Mpa
285,667	286	10,617	7,078	5,308	4,247	3,539	3,033
181,667	182	6,752	4,501	3,376	2,701	2,251	1,929
143,333	143	5,327	3,551	2,664	2,131	1,776	1,522
116,333	116	4,324	2,882	2,162	1,729	1,441	1,235
106,000	106	3,940	2,626	1,970	1,576	1,313	1,126
94,854	95	3,525	2,350	1,763	1,410	1,175	1,007
76,730	77	2,852	1,901	1,426	1,141	951	815

Table 25 –Results from the slot flow approximation for buttress thread

Buttress thread							
Viscosity (cP)	**Viscosity (Pa.s)**	**dp_f/dL (Pa)**					
		20 Mpa	30 Mpa	40 Mpa	50 Mpa	60 Mpa	70 Mpa
285,667	286	317	211	159	127	106	91
181,667	182	202	134	101	81	67	58
143,333	143	159	106	80	64	53	45
116,333	116	129	86	65	52	43	37
106,000	106	118	78	59	47	39	34
94,854	95	105	70	53	42	35	30
76,730	77	85	57	43	34	28	24

CONCLUSIONS AND RECOMMENDATIONS

Conclusions

The various studies of API connections reviewed highlighted important information about the characteristics and functions of connections:

- Normal contact forces and stresses are highest at the ends of the connection
- Stress increased with the number of turns applied during the make up process
- Tensile loads decreases normal contact forces and sealability in thread connections
- Assembly contact pressure increases with increases in internal pressure
- Galling occurs fastest at the ends of the connections
- Thread tolerances affect the number of turns for hand tight connections
- Thread sealability is controlled by the stab flanks as opposed to the load flanks
- Variables such as surface finish, coatings, thread lubricants, and speed of make up can affect torque
- Tension has no effect on torque, while pressure increases the required torque reuired for make up or break out

A survey of many drilling projects done in tight gas reservoirs around the world produced average reservoir properties, which can be used as guidelines when deciding which type of connections to be used. **Table 8** displays the results from the survey.

The average values obtained represent the minimum values API connections should be able to seal. These values can also be used in experiments designed to test the leakage of thread connections, namely the grooved plate method. The experiment can be done under these conditions of temperature and pressure and the results can signify the possible behavior of thread compounds and thread connections in tight gas fields.

A procedure to measure the viscosity of thread compound was established and used to measure the viscosities of three different samples of thread compound at various temperatures. Viscosity values are shown in **Table 26**.

Table 26 –Summary of viscosity results

	Viscosity (cP)		
Temperature (^{0}F)	API Thread Compound	NCS-30	Kopr-Kote
32.9	285,667	260,000	183,333
50.4	181,667	171,333	125,667
67.9	143,333	135,667	101,280
85.8	116,333	111,333	73,168
103.9	106,000	93,002	54,371
121.5	94,854	81,205	47,758
139.5	76,730	69,851	

The data above was fitted to a function and extrapolated to find the viscosity at the average reservoir temperature found from the review of tight gas projects. The viscosities of each of the thread compounds at 256 ^{0}F are shown in **Table 27**. These values represent the expected viscosity of thread compound in tight gas reservoirs.

Table 27 – Viscosity of thread compound at average reservoir temperature

Thread Compound	**Viscosity @ 256 ^{0}F**
API Thread Compound	43114
NCS-30	43512
Kopr-Kote	23508

The thread viscosities found above can be used in conjunction with the slot flow approximation to provide a means of finding a pressure gradient along the grooves of the grooved plate used in the groove plate method. This pressure gradient can be used to simulated results by applying the pressure gradient to

determine leak pressure before the experiment is actually conducted. This can be used as a check of experimental results to validate experimental procedure.

Recommendations

- The measurement of the viscosity of the thread compound samples can be repeated using the average temperatures, which can better represent downhole conditions of tight gas wells.
- The experiment known as the grooved plate method can be carried out using the results from the tight gas reservoirs as test parameters to identify leak parameters of API round thread connections.
- The slot flow approximation can be used as an analytical method to reinforce experimental data or be used instead of conducting lengthy and costly experiments.

REFERENCES

1. Badicioiu, M., and Teodoriu, C., 2007, Sealing Capacity of API Connections- Theoretical and Experimental Results, Paper SPE 106849, presented at the SPE Productions and Operations Symposium, Oklahoma City, Oklahoma, 31 March-3 April.
2. Absill, W., Patillo, P., and Rogers, W.: Investigation of API 8 Round Casing Connection Performance- Part I: Introduction and Method of Analysis, , *ASME Journal of Energy Resources Technology*, **106**, pp 130-136, ASME Paper no. 83-Pet-16.
3. Hoenig, S., and Oberndorfer, M., 2006, Tightness Testing of Environmentally Friendly Thread Compounds, Paper SPE 100220. Presented at the SPE Europe/EAGE Conference, Vienna, Austria, 12-15 June
4. Vega Navarro, O., 2006, Oil Country Tubular Goods Connections Principles, Design Features and Generalities Analysis and Classification of Selected Samples, Technische Universitat Clausthal, Master's thesis.
5. Holditch, S. A., 2006, Tight Gas Sands, Paper SPE 103356. Paper published in the Distinguished Author Series, June.
6. Crotti, M.A., 2007, Water Saturation in Tight Gas Reservoirs, Paper SPE 107145, Presented at the SPE Latin American and Caribbean Petroleum Engineering Conference, Buenos Aires, Argentina, 15-18 April.
7. Lee, W.J., 1982, Well Testing, Society of Petroleum Engineers of AIME, Dallas, Texas, 1982. 80.
8. Dutton S.P., Clift S.J., Hamilton D.S., Hamlin H.S., Hentz T.F., Howard W.E., Akhter M.S., et al., 1993, Major Low-Permeability Sandstone Gas Reservoirs in the Continental United States, Bureau of Economic Geology, University of Texas at Austin, Report of Investigations No. 211, Austin, Texas, 221p.
9. Meckel, L.D., and Thomasson M.R.: Pervasive Tight-gas Sandstone Reservoirs: An Overview, Vail Hedberg Conference: *AAPG Hedberg Series* 13-27.

10. Garbutt, D., Holditch S., Lancaster D., Bryant I., Glaser K., 2004, Unconventional Gas, January, Schlumberger, http://www.slb.com/media/services/solutions/reservoir/uncongas_whitepaper.pdf, downloaded on 02/10/09.
11. Law, Tight Sand Basins, 2003, Advanced Resources International Inc., http://www.adv-res.com/pdf/Tight-Sand-Basins.pdf, downloaded on 02/12/09.
12. Basquet R., Wennberg O.P., Veire H.H., and Ingsøy P., Dynamic Behavior of a Tight Gas Sandstone Reservoir in North Africa, 2007, presentation at PEA Tight Gas Forum, London, 2007.
13. Scott C., Experiences in Developing a Tight Gas Field in Algeria, 2007, Presentation at the PEA Tight Gas Forum, London, June.
14. Gijtenbeek, K., Loidl, H., and Batenburg, D., Hydraulic Fracturing in Deep Horizontal Wells in Germany, Power-point presentation.
15. Wolhart, S.L., Berumen, S., Cipolla, C.L., Barton, C.A., and Branagan, P.T., 2000, Use of Hydraulic Fracture Diagnostics to Optimize Fracturing Jobs in the Arcabuz-Culebra Field, Paper SPE 60314 presented at the SPE Rocky Mountain/Low Permeability Resevoir Symposium and Exhibition Denver, Colorado, March.
16. Dennison, D., "Drilling of a Natural Gas Well and Natural Gas Production in the Piceance Basin," Garfield County Oil & Gas Liaison, http://www.garfield-county.com/docs/drilling_101.pdf, downloaded on 07/15/2008.
17. Western Gas Resources and EPA's Natural Gas STAR Program, 2006, Williams Experience in Methane Emissions Mitigation, Producers and Processors Technology Transfer Workshop, May.
18. Weimer, R.J., Sonnenberg S.A., and Young G.B.C., Wattenberg Field, Denver Basin, Colorado, Published in AAPG # 20001.
19. Holditch, S.A., Lin Z-S., and Spivey, J.P., 1991, Estimating the Recovery from an Average Well in a Tight Gas Formation, Paper SPE 21500. Presented at the SPE Gas Technology Symposium, Houston, Texas, January.
20. Meeks, M.H., Susewind, K.D., and Templeman, T.L., 2006Maximizing Gas Recovery From Tight Gas Reservoirs in Trawick Field, Paper SPE 101221. Presented at the Abu Dhabi International Petroleum Exhibition and Conference, Abu Dhabi, U.A.E., November.

21. McCoy, A.W., Davis, F.A., Elrod, J.P., Rhodes, S.L., Singh, S.P., 1996, Using Horizontal Well Technology for Enhanced Recovery in Very Mature, Depletion Drive Gas Reservoirs – Pirkle #2 Well, A Case History, Carthage (Lower Petit) Field, Panola County, Texas, Paper SPE 36751. Paper presented at SPE Annual Technical Conference & Exhibition held in Denver, Colorado October.
22. Guangjie, Y. Zhenqiang, Y. Qinghua, and W. Zhentong, T., 2006, Numerical and experimental distribution and stress fields in API round threaded connection, Science Direct, February, http://www.sciencedirect.com/science?_ob=MImg&_imagekey=B6V2X-4J7B16W-4-14&_cdi=5714&_user=952835&_orig=search&_coverDate=12%2F31%2F2006&_sk=999869991&view=c&wchp=dGLbVtz-zSkWb&md5=29a4c2d1c5bcf5498a157c5a4d5e6af9&ie=/sdarticle.pdf, downloaded on 02/01/08
23. Asbill, W. Patillo, P., and Rogers, W., 1984, Investigation of API 8 Round Casing Connection Performance- Part I: Introduction and Method of Analysis, ASME Paper no. 83-Pet-16, *ASME Journal of Energy Resources Technology*, **106**, 130-136.
24. Asbill, W. Patillo, P., and Rogers, W., 1984, Investigation of API 8 Round Casing Connection Performance- Part II: Stresses and Criteria, ASME Paper no. 83-Pet-17, *ASME Journal of Energy Resources Technology*, **106**, 137-143.
25. Asbill, W. Patillo, P., and Rogers, W., 1984, Investigation of API 8 Round Casing Connection Performance- Part III: Sealability and Torque, ASME Paper no. 83-Pet-18, *ASME Journal of Energy Resources Technology*, **106**, 144-154.
26. Bourgoyne Jr., A.T., Chenevert, M.E., Millheim, K.K., and Young Jr., F.S., 1986, Applied Drilling Engineering, 1986, SPE Textbook Series, **Vol**. 2.
27. Brookfield Engineering Laboratories, Inc., Brookfield DV-III Ultra Prorammable Rheometer Operating Instructions Manual No. M/98-211-B0104, Middleboro Massachusettes.
28. Jet Lube of Canada Ltd, API Modified Thread Compound, http://www.jetlubecanada.com/api.pdf, downloaded on 04/14/2009.
29. Jet Lube of Canada Ltd, NCS-30 thread compound, http://www.jetlube.com/jetlube/uploads/pdf/msdspdf/ncs30of.pdf, downloaded on 04/14/2009.

30. Jet Lube of Canada Ltd, Kopr-Kote, http://www.jetlubecanada.com/Kopr-Kote%20T.pdf, downloaded on 04/14/2009.
31. Artisan Scientific, Brookfield Refrigerated Temperature Bath, http://www.artisan-scientific.com/ViewImage.aspx?Image=Brookfield_TC500_View1.JPG&Item=57894, downloaded on 05/19/09.
32. H&C Thermal Systems, Thermolyne Furnace 30400**,** http://www.affordablelabovens.com/product_ctg.asp?products=54&Premium_Large_Muffle, downloaded on 05/19/09.

NOMENCLATURE

α = stabbing flank angle

API = American Petroleum Institute

ASTM = American Society of Testing and Materials

β = load flank angle

Bcf = billion cubic feet

BHA = bottom-hole assembly

COD = coupling outer diameter

D = non-Darcy flow constant

$\frac{dp_f}{dL}$ = pressure gradient

e_w = weight gain or loss due to end finishing, lb

FEM = Finite Element Method

γ = tooth angle

h_1 = net pay thickness

h_2 = depth of grooves

ID = inner diameter

JR = James Reservoir

k = permeability

L = length of pipe including end finishing, ft

μ_1 = friction coefficient

μ_2 = viscosity of thread compound

$\mu_{\bar{p}}$ = fluid viscosity

Mcf = 1000 cubic feet

MCFD = 1000 cubic feet per day

mD = milli Darcy

MD = measured depth

MMCFD = million cubic feet per day

MUL = make up loss

N_L = length of coupling

OCTG = Oil Country Tubular Goods

OD = outer diameter

PB = Piceance Basin

pwf = flowing pressure

$\bar{p}$ = average reservoir pressure

q = maximum allowable leak rate

q_g = flow rate

r = radius of integration point

r_e = drainage radius

r_w = wellbore radius

s = skin factor

σ_{nn} = normal contact stress

T = reservoir temperature

t = wall thickness

Tcf = trillion cubic feet

TVD = true vertical depth

W = width of grooves, m

WB = Wattenberg Field

w_L = calculated weight of a pipe L, lb

w_{pe} = plain end weight, lb/ft

$z_{\bar{p}g}$ = z factor

APPENDIX A

Slot Flow Approximation

This approximation was initially designed to represent annular flow by flow through rectangular slots because rectangular slot flow equations are much simpler to use. It is calculated to be reasonably accurate when $d_1/d_2 > 0.3$. **Fig. 53** shows the transition from annular flow to slot flow by rearranging the shape of the system.

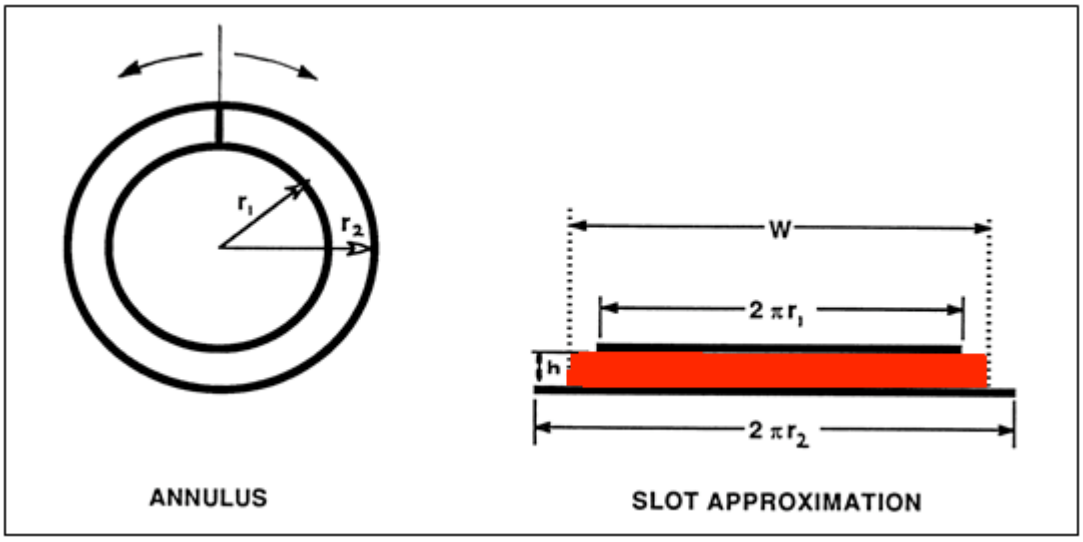

Fig. 53 – Transformation from annular flow to slot flow (modified from Bourgoyne et. al)

The dimension of the region of interest is given by **Eq. 7, 8 and 9**[26]**.**

$$A = Wh = \pi\left(r_2^{\,2} - r_1^{\,2}\right) \quad \text{(7)}$$

$$h = r_2 - r_1 \quad \text{(8)}$$

$$W = \pi\left(r_2 + r_1\right) \quad \text{(9)}$$

Taking an element of fluid in the slot as shown in **Fig. 54** we sum forces acting on it. **Eq. 10, 11, 12, and 13**[26] shows the forces acting on each face of that element due to fluid pressure.

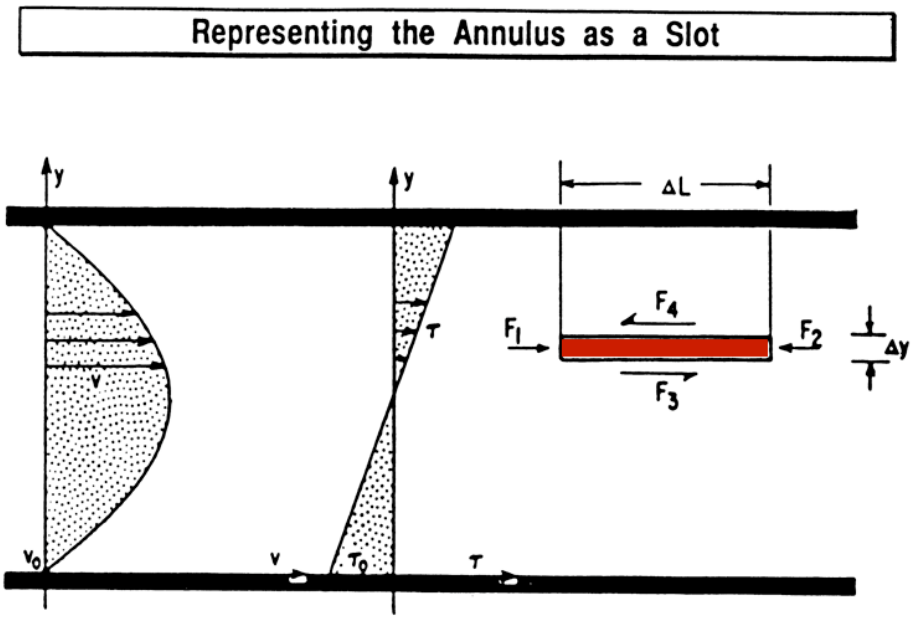

Fig. 54 – Free body diagram for fluid element in a narrow slot[26]

$$F_1 = p \times W \times \Delta y \quad \text{..... (10)}$$

$$F_2 = p_2 \times W \times \Delta y = \left(p - \frac{dp_f}{dL} \Delta L \right) \times W \times \Delta y \quad \text{..... (11)}$$

$$F_3 = \tau \times W \times \Delta L \quad \text{..... (12)}$$

$$F_4 = \tau_{y+\Delta y} \times W \times \Delta L = \left(\tau + \frac{d\tau}{dy} \Delta y \right) \times W \times \Delta L \quad \text{..... (13)}$$

The sum of these forces for stead flow must equal to zero shown by **Eq. 14**[26]

$$F_1 - F_2 + F_3 - F_4 = 0$$

$$p W\Delta y - \left(p - \frac{dp_f}{dL}\Delta L \right) W\Delta y + \tau W\Delta L - \left(\tau + \frac{d\tau}{dy}\Delta y \right) W\Delta L = 0 \quad \text{..... (14)}$$

Simplifying this equation by expanding and dividing throughout by $W\Delta L\Delta y$ gives **Eq. 15**[26]

$$\frac{dp_f}{dL} - \frac{d\tau}{dy} = 0 \quad \text{..... (15)}$$

Integrating with respect to y and separating variables we get **Eq. 16**[26], where τ_0 is the constant of integration and is the shear stress when y=0

$$\tau = y\frac{dp_f}{dL} + \tau_0 \quad \text{..... (16)}$$

Shear rate to be used from her on will be designated as **Eq. 17**[26]

$$\dot{\gamma} = -\frac{dv}{dy} \quad \text{..... (17)}$$

Now substituting in Newtonian model, **Eq. 18**[26] gives

$$\tau = \mu\dot{\gamma} = -\mu\frac{dv}{dy} = y\frac{dp}{dL} + \tau_0 \quad \text{..... (18)}$$

By separating and integrating we find an equation for fluid velocity. **Eq. 19**[26] shows this equation with v_0 being a constant of integration.

$$v = -\frac{y^2}{2\mu}\frac{dp_f}{dL} - \frac{\tau_0 y}{\mu} + v_0 \quad \text{..... (19)}$$

Using the assumption that the fluid wets the pipe walls the boundary conditions for **Eq. 20** becomes y = 0 and y = h. Substituting in **Eq. 19** makes $v_0 = 0$ and **Eq. 20**[26] shows the value of τ_0

$$0 = -\frac{h^2}{2\mu}\frac{dp_f}{dL} - \frac{\tau_0 h}{\mu} + v_0$$

$$\tau_0 = -\frac{h}{2}\frac{dp_f}{dL} \quad \text{..... (20)}$$

The values of v_0 and τ_0 were then substituted in **Eq. 19** to produce an equation of v shown in **Eq. 21**[26]

$$v = \frac{1}{2\mu}\frac{dp_f}{dL}\left(hy - y^2\right) \quad \text{..... (21)}$$

The flow rate is found by integrating with respect to area from 0 to h. The result is shown in **Eq. 22**

$$q = \int_0^h v dA = \int_0^h v W dy = \frac{W}{2\mu}\frac{dp_f}{dL}\int_0^h \left(hy - y^2\right) dy$$

$$q = \frac{Wh^3}{12\mu}\frac{dp_f}{dL} \quad \text{..... (22)}$$

VITA

Name:	Dwayne Bourne
Permanent Address:	Texas A&M University, Department of Petroleum Engineering 3116 TAMU College Station, Texas, 77843-3116
Email:	dborn1@hotmail.com
Education:	B.S., Physics South Carolina State University USA, 2007 M.S., Petroleum Engineering, Texas A&M University, USA, 2009
Member:	Society of Petroleum Engineers